Techno-economic analysis of ammonia cracking for large scale power generation

International Journal of Hydrogen Energy 71 (2024) 571–587

Contents lists available at ScienceDirect

International Journal of Hydrogen Energy

journal homepage: www.elsevier.com/locate/he

Techno-economic analysis of ammonia cracking for large scale power generation

Simon Richard [a,b], Alvaro Ramirez Santos [a], Pierre Olivier [a], Fausto Gallucci [b,*]

[a] ENGIE Lab CRIGEN, 4 rue Joséphine Baker, Stains, France
[b] Sustainable Process Engineering, Chemical Engineering and Chemistry, Eindhoven University of Technology, Den Dolech 2, 5612, AZ, Eindhoven, the Netherlands

ARTICLE INFO

Handling Editor: Prof I Tolj

Keywords:
Power generation
Ammonia
Membrane reactor
Combined cycle gas turbine

ABSTRACT

The increasing interest in leveraging green ammonia to mitigate carbon emissions in fertilizer production is paralleled by an expanding acknowledgment of its potential as a fuel for decarbonizing the electricity sector, particularly in high-efficiency gas turbine power plants. Co-firing ammonia with hydrogen presents a promising method for integrating ammonia into existing infrastructures. Within this context, the development of efficient technology for ammonia cracking presents a potential avenue for deploying ammonia in gas turbines. The objective of this study is to conduct a preliminary techno-economic evaluation and uncertainty analysis of two cracking technologies namely a membrane reactor and a conventional FTR (Fired Tubular Reactor) for the co-firing of ammonia with hydrogen in a CCGT (Combined Cycle Gas Turbine) plant. The integration of a membrane reactor during the cracking stage demonstrates a remarkable improvement in the system's thermal efficiency, surpassing traditional approaches by over 25%. Additionally, it brings about an approximate 10% reduction in the levelized cost of hydrogen (LCOH), despite a higher initial capital expenditure (CAPEX). At the CCGT level, the discrepancy in levelized cost of electricity (LCOE) narrows, as it is strongly influenced by the cost of ammonia constituting 80% of the LCOE. Beyond LCOE, the widespread adoption of these systems also faces challenges due to material scarcity. Analysis reveals that revamping just 1 GWe of CCGT assets using membrane reactors would for example necessitate approximately 0.11% of the global palladium supply, and 10% of the global ruthenium production. Considering the limited availability of these resources, coupled with their high demand across multiple sectors and the possibility of external factors such as geopolitical tensions, this strategy seems unfeasible. To tap into this market, future research should prioritize the exploration of alternative membrane materials, such as carbon molecular sieves, and catalysts, like nickel.

Nomenclature

ACM	Aspen Custom Modeler
BOP	Balance of Plant
CCF	Capital Charge Factor
CFD	Computational Fluid Dynamic
C&OC	Owner's and contingencies costs
CCGT	Combined Cycle Gas Turbine
CP	Concentration Polarization
EU	European Union
FTR	Fire Tubular Reactor
GHG	Green House Gas
GHSV	Gas hourly Space Velocity
GT	Gas Turbine
HRF	Hydrogen Recovery Factor
HRGS	Heat Recovery Steam Generators
HP	High Pressure
IC	Indirect Costs
IP	Intermediate Pressure
IEA	International Energy Agency
LCOH	Levelized Cost of Hydrogen
LCOE	Levelized Cost of Electricity
LHV	Lower Heating Value
LP	Low Pressure
MR	Membrane Reactor
MTPD	Metric ton per day
NOX	Nitrous oxide
NG	Natural Gas
NGCC	Natural Gas Combined Cycle
OEM	Original Equipment Manufacturer
OD	Outer diameter

(continued on next column)
(continued)
(continued on next page)

* Corresponding author.
E-mail address: F.Gallucci@tue.nl (F. Gallucci).

https://doi.org/10.1016/j.ijhydene.2024.05.308
Received 3 November 2023; Received in revised form 9 May 2024; Accepted 19 May 2024
Available online 22 May 2024

(*continued*)

PBMR	Packed bed membrane reactor
PSA	Pressure swing adsorption
SMR	Steam Methane Reforming
SQRP	Sequential Quadratic Programming
TRL	Technology Readiness Level
TEC	Total equipment cost, €
TIC	Total Installation Cost, €
TR	Traditional Reactor
TPC	Total Plant Cost, €
VRE	Variable Renewable Energy

Symbol		
k_0	Pre exponential factor	$mol\, m^{-2} s^{-1} bar^{0.5}$
n	Exponential factor in permeation law	–
F	NH_3 Molar flowrate	kmol hr^{-1}
E_a	Activation Energy	kJ mol^{-1}
R	Universal gas constant	J $K^{-1} mol^{-1}$
Pe_{0,H_2}	Permeability	$[mol\, m^{-1} s^{-1} Pa^{-0.5}]$
P	Pressure	Bar
T	Temperature	°C
W	Weight of catalyst	kg

Greek Letter		
ϵ	Bed voidage	–
η_{th}	Thermal efficiency	–
δ	Membrane Thickness	[m]

Subscript and Superscript	
m	Membrane
Perm	Permeate
Ret	Retentate
Aux	Auxiliary
In	Input

1. Introduction

The depletion of fossil fuels, coupled with increasing concerns about climate change, is currently driving the substitution of conventional technologies and energy sources with renewables and innovative strategies to meet the growing global energy demand. Variable Renewable Energy (VRE) adoption has surpassed 40% in regions such as California [1], Denmark, and South Australia [2]. Likewise, in the coming years, numerous countries are expected to see a substantial increase in the integration of VRE into their energy systems. The International Energy Agency(IEA)Stated Policies Scenario actually predicts that the share of renewables would rise from 26% in 2018 to 44% in 2040, while the Net Zero by 2050 scenario envisions almost 90% of electricity generation coming from renewable sources [3].

To tackle the inherent intermittency of renewable energy and mitigate curtailment, "power-to-liquid" and "power-to-gas" technologies exhibit substantial potential. These technologies not only tackle the intermittency issue but also provide a viable solution for generating fossil-free resources. This, in turn, can cater to demanding sectors that pose challenges in terms of electrification. By embracing Power-to-X fuels, traditional power generation, particularly combined cycle gas turbines (CCGTs) with their unmatched efficiency at large scale and reasonable flexibility, could make substantial contributions to creating a greener energy landscape while facilitating the shift towards VRE [4]. This improvement plays a pivotal role in preventing carbon entrenchment and minimizing costly asset devaluation during the transition to a decarbonized grid [2]. The initial stages of this journey have been characterized by the incorporation of hydrogen blending in gas turbines, with gas turbine OEMs (original equipment manufacturers) recognizing the viability of incorporating up to 60 vol% hydrogen in specific existing turbine types. According to a report by ETN Global [4], some OEMs are now aiming to increase this ratio to 100 vol % hydrogen. However, the widespread adoption of hydrogen as an energy carrier still faces substantial challenges, notably in the domains of transportation, storage, and the possibility of potential leaks [5–7].

In contrast, green ammonia has emerged as a remarkable zero-carbon alternative, primarily due to its dispatchability and relative ease of storage at high volumes [8]. Liquid ammonia offers several advantages, including a notably high hydrogen storage density, with a weight percentage of 17.8% by mass and a volume of 121 kg-H_2/m^3. This exceeds the densities achieved by other advanced hydrogen storage systems or hydrogen-containing material, including metal hydrides (25 kg-H_2/m^3), liquefied hydrogen (71 kg-H_2/m^3) [9], compressed hydrogen at 700 bar (42.2 kg-H_2/m^3) [9], methanol (99 kg-H_2/m^3) [9], or formic acid (53 kg-H_2/m^3) [10]. The increased hydrogen carrying capacity per unit volume of ammonia translates into a lower cost per unit of stored energy compared to alternative options [11–13]. For example, Zhao et al. (2019) [12] found that ammonia has the lowest global cost (including production, storage, and transportation) being 31% lower than compressed hydrogen. Dias et al. (2020) [13] indicated that storing hydrogen as a gas is costlier, with storage costs 46% higher than ammonia. The IEA [14] nuanced those finding by suggesting that hydrogen gas could be the best option for inland transport up to 3500 km, after which ammonia becomes more economical. Ammonia is also advantageous due to well-established standards, a long history of safety, and a storage and distribution infrastructure that has been in place for more than 75 years [15]. These numerous advantages have sparked a growing interest in utilizing ammonia as a carbon-free fuel for gas turbines, as evidenced by the increasing number of research papers dedicated to exploring this field, as depicted in Fig. 1.

However, the combustion characteristics of ammonia differ significantly from those of traditional hydrocarbon and hydrogen fuels, posing certain challenges. One major concern is the relatively low flame speeds of ammonia-air mixtures, which are only one-fifth of those observed in methane-air mixtures at 298 K and 0.10 MPa [16,17]. Moreover, ammonia is a toxic substance, and the emission of unburned ammonia from gas turbines is undesirable. The presence of nitrogen oxides (NOx), unburned species like NH_3, and trace amounts of hydrogen further complicate matters in this field. While direct combustion has been studied, it requires the development of new fuel delivery systems, modifications to gas turbine enclosures, and rethinking the design of NOx treatments and combustors [4,15]. Numerous OEMs are currently involved in prototype development in this field. Notably, Mitsubishi Heavy Industries (MHI) which aims to create an industrial-scale turbine (50 MW) by 2025–2030 [18]. In 2021, IHI partnered with GE (General Electric) to produce gas turbines with the goal of achieving 100% ammonia-based combustion by 2030 [19].

To overcome the challenge posed by the low burning velocity of ammonia and enable its use with existing industrial devices, alternative studies explore its use as a co-fuel, often in conjunction with hydrogen [20,21] or methane (although the latter emits carbon dioxide) [22]. Research as early as the 1960s [23] demonstrated that combining ammonia's slow flame with hydrogen's fast, hot flame can produce combustion properties comparable to methane in a gas turbine. A blend with 30% H_2 (vol. %) seems to have gained attention in this field but uncertainties still remain regarding safe, stable, and efficient operation while minimizing NOx emissions. Numerous studies have been conducted on the combustion and emissions performance of ammonia/hydrogen blends [17,24–32]. For instance, Pugh et al. (2019) [26] highlighted the benefits of reactant humidification in reducing NOx emissions and recommended a 70/30% NH_3/H_2 mix for optimal stability, mimicking the behavior of a premixed CH_4 flame. Hussein et al. (2019) [25] identified a 60/40% NH_3/H_2 ratio as ideal for minimizing unburned ammonia and achieving high flame temperatures, despite high NO emissions. Hu et al. (2024) [31] reached a parallel conclusion, noting optimal emissions of unburned NH_3, NO_2, and N_2O at stoichiometric conditions, with NO emissions decreasing under rich-burn conditions. Finally, Yan et al. (2023) [32] noted that a minimum of 20% hydrogen addition was necessary for effective operation, although it did not match the combustion rates of gasoline or methane. They suggested that natural gas engines, with higher compression ratios, are better

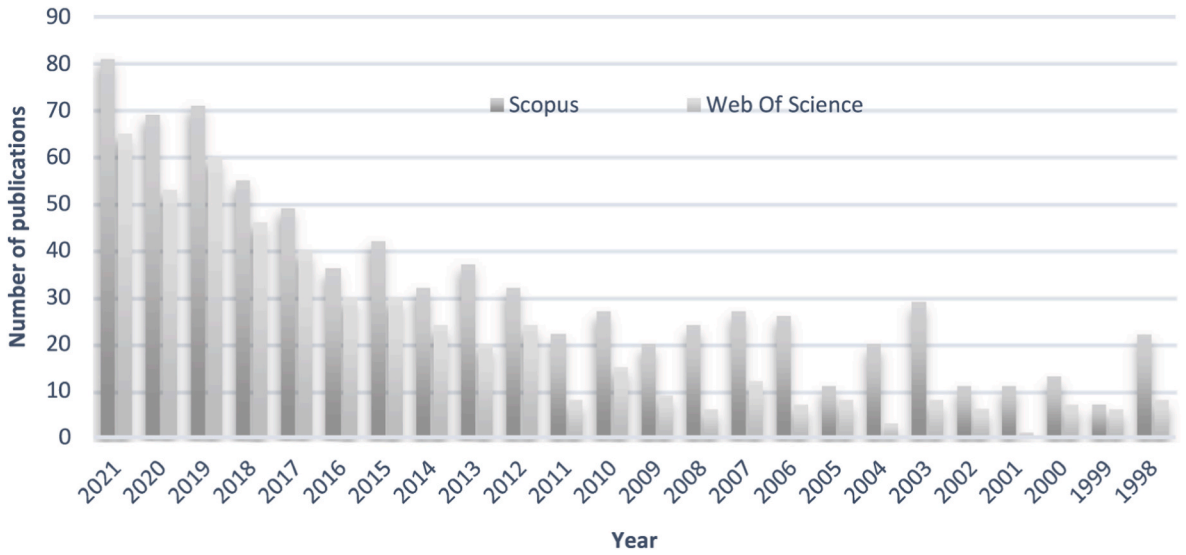

Fig. 1. Number of scientific articles mentioning the key words "Turbine" and "Ammonia" in their abstract from Scopus and Web of Science.

suited for ammonia-hydrogen use and recommended avoiding lean operation in spark ignition engines with ammonia.

Hydrogen enhances ammonia combustion as a carbon-neutral option by compensating for ammonia's lower reactivity and flame speed. Yet, retrofitting existing combined-cycle gas turbine (CCGT) assets with imported ammonia fuel requires on-site catalytic decomposition, presenting another challenge. Although ammonia cracking has not gained commercial popularity in the past, there is currently a significant drive to develop ammonia cracking facilities. This drive is reinforced by various recent industrial press releases promising the construction of large-scale central facilities to generate hydrogen from imported ammonia in the near future [33–36]. This process traditionally relies on a high-temperature reactor followed by a separation system to effectively extract hydrogen. To achieve complete conversion, the ammonia cracking process normally runs at temperatures exceeding 700 °C and frequently makes use of nickel as a catalyst. However, precious metal catalysts like rhodium, iridium, platinum, and especially ruthenium demonstrate better catalytic activity in this process [9,37–39]. Hydrogen recovery is commonly accomplished using Pressure Swing Adsorption (PSA), although cryogenic separation and ion-exchange zeolites are also viable alternatives [40].

In response to the challenges posed by cracking reaction temperature and the subsequent separation of unreacted gases in traditional systems, researchers have explored the use of membrane reactors (MR) to efficiently recover the H_2 stored in NH_3. The direct removal of H_2 within the catalytic bed, where chemical reactions take place, not only surpasses the thermodynamic limitations of the traditional process but also lessens the need for downstream product purification. Among different types of membranes, Pd-based membranes are generally considered the most suitable due to their favorable balance of permeance, selectivity and stability towards hydrogen [40]. Several researchers have already proven and highlighted the benefit of this arrangement at laboratory scale. For instance, Cechetto et al. (2021) [41] conducted experiments that showed up to a 50% increase in conversion rates achievable with a Pd-based membrane reactor compared to a traditional reactor utilizing (2 wt%) Ru/Al_2O_3. Similarly, Itoh et al. (2014) [42] demonstrated that a Pd membrane inserted in a (2 wt%) Ru/Al_2O_3 could increase ammonia conversion rates by up to 15%. In a similar vein, Liu et al. (2020) [43] found that a stainless-steel supported palladium based membranes could enhance conversion by up to 30%, with a successful 200 h test. According to their research, Park et al. (2020) [44] found that in situ H_2 extraction increased H_2 productivity by more than 63% when compared to a TR. This observed increase in NH_3 conversion with membrane reactor can be explained in two ways: either by shifts in thermodynamic equilibrium or, alternatively, as a kinetic enhancement due to the selective separation of H_2 from the reaction products that, in the absence of this in-situ separation, would have an inhibitory effect on the forward kinetics of the NH_3 decomposition reaction [42,45].

Several studies have also conducted economic analyses of this process, focusing on both traditional systems and, occasionally, membrane reactor systems. For instance, Lim et al. (2022) [46] discovered that the membrane reactor could lead to an 11% cost reduction at 300 kg-H_2 per day and a 14% reduction at 900 kg-H_2 per day, with an efficiency of 82.7% and 78.7%, respectively. Moreover, greenhouse gas emissions were reduced by approximately 17%, from 5.4 to 4.5 kg_{CO2}-eq/kg-H_2. Makhloufi et al. (2021) [47] designed a large-scale Ammonia-to-Hydrogen plant that operates at a thermal efficiency of 68.5% and produces 200 ton per day of pure hydrogen at 250 bar. The authors utilized a fire tubular reactor (FTR), a technology akin to traditional reformer technology seen in steam methane reforming, which involves vertical catalyst-filled tubes within a firebox, where radiant heat is transferred to the process tubes. The estimated LCOH (Levelized Cost Of Hydrogen) was about 4.82 €/kg with a base green ammonia cost of 450 €/ton. Nasharuddin et al. (2019) [48] estimated the levelized cost of H_2 to be 4.70 €/kg at a capacity of 1000 ton per day. They also noted that the cost of H_2 is closely linked to the feedstock price of NH_3, which varies between 3.00 and 6.28 €/kg when the NH_3 price is modified by ±75%. At the power plant level, Cesaro et al. (2021) [49] forecasted the price of electricity from green ammonia to be 167–197 $/MWh at 25% power plant capacity factor.

Although there has been a recent increase in research conducted by many scholars on the subject of ammonia cracking and ammonia combustion, still a small number of papers have focused on the economic analysis aspect and even fewer are dedicated to ammonia cracking for power generation applications CCGTs. The present study aims at investigating from an economic viewpoint the potential to use large scale ammonia cracking facility to generate hydrogen from imported ammonia at the capacity required for a CCGT. The novelty of this study lies in the comprehensive modeling and techno-economic assessment of the membrane reactor technology specifically designed for this application. The study also includes a comparison with a more conventional process like the currently available SMR technology. (cf. Fig. 2).

2. Material and methods

To achieve the objective, steady-state simulations were conducted in

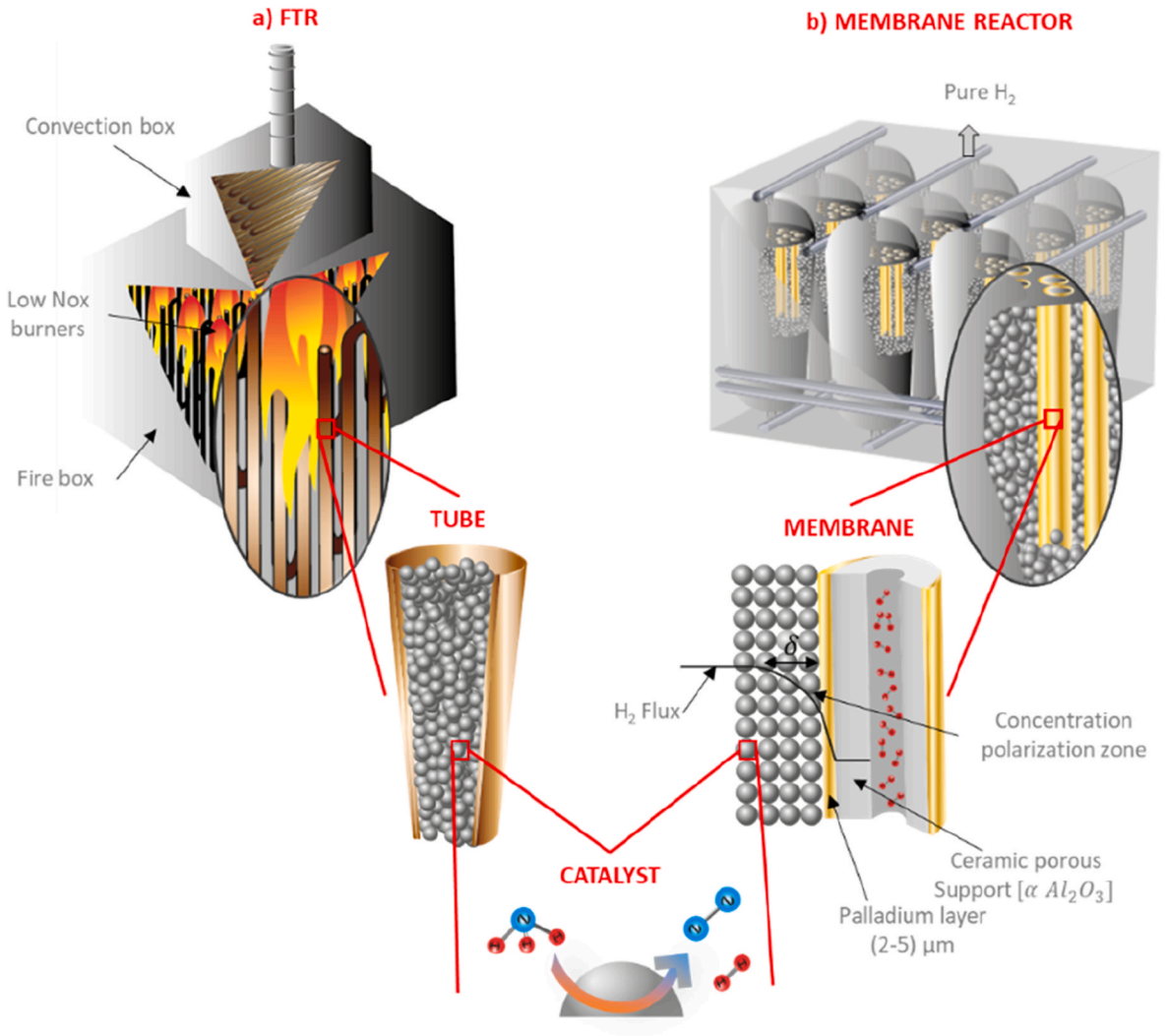

Fig. 2. Sketch illustrating the two reactors under consideration in this study a) FTR and b) MR.

Aspen Plus™ v11. These simulations provided the required inputs for a techno-economic evaluation. The Peng Robinson equation of state was employed, and the NRTL method was utilized for the absorption section. The membrane reactor was coded in Aspen Custom Modeler™ (ACM), allowing for seamless integration with Aspen Plus™ flowsheets as a custom component. This software has embedded methods to retrieve thermodynamic properties and employs a coding syntax similar to Visual Basic.

2.1. Layouts descriptions and general assumptions

This section outlines the process layouts depicted in Fig. 3. The reference NGCC (Natural Gas Combined Cycle) power plant is representative of Amercoeur Power Plant located in Belgium utilizing a single large-scale gas turbine (GT) "F class" (General Electric 9FB) with a gross power output of approximately 310 MW. It also includes a heat recovery steam generator (HRSG) and a single steam turbine in a dual-shaft configuration, featuring two alternators for the steam turbine and gas turbine. The plant receives natural gas at 30 bar and 27 °C and has a net power output of 420 MW. The steam turbine comprises high-pressure (HP), intermediate-pressure (IP), and low-pressure (LP) turbine, with extraction points for regenerative heating of feedwater and condensate. Additionally, this study considers a carbon dioxide recovery facility based on conventional ethanolamine absorption.This particular section is however not modeled and is solely considered from an efficiency & techno-economic perspective assuming that this process is at best 90–95% effective at capturing emissions as already reported [49] and that the amount of energy for regeneration of the solvent is assumed equal to 3.95 GJ/t CO_2 with steam at a pressure of 4.0 bar according to previous literature [50]. The CO_2 released in the stripper column is compressed in an intercooled compressor and, after reaching liquid phase liquefaction in the 80 bar aftercooler, pumped to the delivery pressure fixed at 110 bar.

Regarding the retrofits with ammonia, a mixture consisting of 30% hydrogen (H_2) by volume is adopted, which aligns with existing literature [17,24–30]. In this scenario, the parameters set for the natural gas (NG) turbine are utilized, and a design specification is put in place to achieve the targeted fuel blend flow rate. This ensures that the power output matches that of its natural gas-based counterpart. This translates to a hydrogen need of 2600 kmol/h at 30 bar. This assumption serves as a fundamental premise for this study. Furthermore, it is crucial to ensure that the temperature remains below 1400 °C to prevent any potential damage to the stainless-steel tubes. Further details on modeling both traditional and retrofitted combined-cycle gas turbine (CCGT) systems with hydrogen-ammonia blends in Aspen Plus are available in Supplementary Materials S1 and S2.

To generate the necessary hydrogen amount for the blend, this study primarily evaluates two cracking technologies: a fire tubular reactor (FTR) and a membrane reactor (MR) process. The system layouts for these technologies can be viewed in Fig. 3. These two processes are

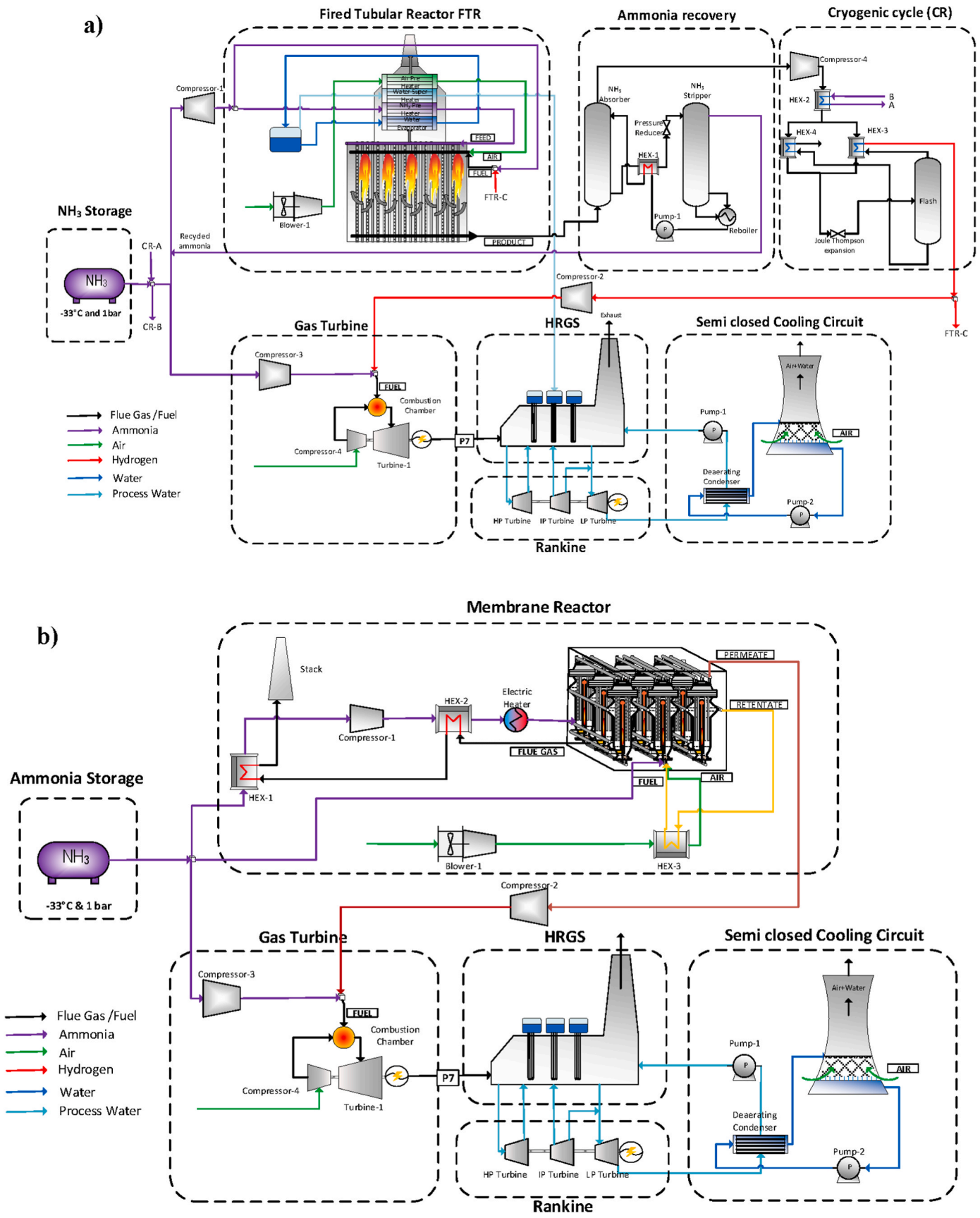

Fig. 3. Process layouts: a) FTR b) MR.

assumed decoupled (i.e. no heat integration) from the power production island which seems beneficial from the point of view of flexibility, and more realistic from the point of view of retrofitting existing assets. In adequation with current practice for large scale storage [51], ammonia is stored at 1 bar and −33 °C in insulated tanks in which the temperature is kept down by slow vaporization, and the ammonia vapor is continually compressed back to a liquid. It is also important to consider that ammonia poses safety and health risks and is corrosive, necessitating that storage containers be constructed or lined with resistant materials, such as stainless steel, which increases both the cost and complexity of storage solutions. However, with over a century of production experience, the technologies and standards for storing, transporting, safely handling, and industrially using ammonia are mature and well-established.

The FTR technology is based on conventional 'reformer' technology (vertical catalyst filled tubes in a firebox with radiant heat transfer to the process tubes) as employed in conventional steam methane reforming. The theoretical combustion study of ammonia with air is carried out by using Gibbs reactor model in Aspen Plus V.11. The 'RPlug' model is adopted to model the reactions tubes. In this work a parabolic distribution of the heat flux is assumed similar to the one outlined in Makhloufi et al. (2021) [47] This distribution is generally influenced by variables difficult to simplify in a model, such as heat release rate, burner configuration, radiation properties, and the geometry of the heater.To retrieve any uncracked ammonia present in the gas, an absorption/desorption process has been designed based on the flow rate, pressure, and temperature of the process gas. In this process, water is utilized as the absorbent, taking advantage of ammonia's high solubility in water. To regenerate the water, a stripping column is employed to evaporate the ammonia. The evaporated ammonia is subsequently cooled and pressurized, allowing it to be recycled back to the cracking step. Regarding purification, a cryogenic separation scenario is favored over the PSA scenario due to the inherent impracticality and safety complications of vast quantities of H_2 storage vessels in pressurized conditions of 200 bar. First the cracked gas is compressed to 240 bars in a 6-stage compressor with intermediate cooling, this is followed by a series of 3 fin plate heat exchangers used to decrease the temperature of the mixture. A Joule-Thomson valve is used to expand the gas mixture to near atmospheric pressure achieving temperature near −230 °C which enables a nearly complete liquefaction of nitrogen [47].

The solution involving the membrane reactor employs a modular design, comprising a series of interconnected units. Scaling up membrane reactors can be done by connecting membranes in series to create longer ones. However, this method faces difficulties with traditional ceramic supports, mainly due to potential seal leakage issues. Alternatively, metallic-supported membranes used in a modular setup are promising, providing an effective way to scale up membrane reactors. To ensure a steady inlet temperature, an electric heat exchanger is installed at the reactor's entrance. The retentate stream, which contains unconverted ammonia and unrecovered hydrogen, is throttled and used to provide the necessary heat for the endothermic cracking reaction. Additionally, ammonia is added as a fuel to ensure the energy balance is maintained when the energy from the retentate stream alone is insufficient to both supply heat to the reactor and pre-heat the reactant. The permeate exits the reactor at atmospheric pressure and is subsequently compressed to the delivery pressure necessary for the combined-cycle gas turbine (CCGT), which is 30 bar. It is then mixed with ammonia to achieve the desired blend composition. To optimize the process, various process parameters have been modified (e.g. temperature, pressure, feed flowrate …), as discussed in subsequent sections. It is important to mention that this study does not cover NOx treatment, which would be essential for practical applications. Most of the assumptions related to the heat exchangers, reactor conditions, CO2 process unit for compression and purification as well as steam cycle and turbomachines efficiencies are presented in Table 1.

Table 1
Main assumptions.

Parameters	Unit	value
Reactors operating conditions		
Reactor inlet temperature	°C	400–460
Pressure reaction side	Bar	10–25
Permeate pressure	Bar	1
CCGT Gas turbine		
Gas turbine power gross power	MW	280
Turbine inlet temperature	°C	1360
Pressure ratio	[−]	18
Turbine isentropic efficiency	%	0.87
Compressor isentropic efficiency	%	0.85
NH_3–H_2 blend composition	% (vol)	30
CCGT Steam cycle		
Steam evaporation pressure	bar	130, 28, 4
Condenser pressure	bar	0.0509
Pinch point ΔT (HP, IP, LP)	°C	50,30,10
Cooling water blowdown from ST condenser cooling tower	t/hr	109,9
Blow down from HRSG drums	t/hr	2,9
CO_2 compression		
Final delivery pressure	bar	110
Compressor isentropic efficiency	%	85
Electrical and auxiliaries		
Driver efficiency	%	95
Generator efficiency	%	98.5
Mechanical efficiencies	%	99.6
Heat exchangers		
Design Minimum ΔT in exchanger gas water	°C	15
Minimum ΔT in exchanger gas gas	°C	30
Heat transfer coefficient gas/gas	W/ m^2/K	60
Heat transfer coefficient gas/liquid	W/ m^2/K	70
Pump and compressor		
Pump isentropic efficiency	%	70
Pump Motor mechanical efficiency	%	85
Compressor/fan/blower isentropic efficiency	%	70
Compressor/fan/blower motor mechanical efficiency	%	85
Natural Gas for the reference CCGT case		
Molar composition	%	CH_4 89.00, C_2H_6 7.00, C_3H_8 1.00, C_4H_{10} 0.11, CO_2 2.00, N_2 0.89
LHV	MJ/kg	46.482

2.2. Reactor and kinetic modelling

In this study, the membrane reactor model is described taking into account material and energy balance through linear differential equations. These equations are discretized along the axial length of the reactor. The model assumes steady-state conditions and negligible radial dispersion. To solve these equations, the Euler method implemented in ACM is utilized. To simulate the hydrogen flux across a Pd-based membrane, an equation based on the Richardson equation is used for each infinitesimal membrane element, as expressed in Eq. (1).

$$J_{H_2} = \frac{Pe}{\delta}\left(p^{n}_{H_{2,ret}} - p^{n}_{H_{2,perm}}\right)\left[\frac{mol}{s\ m^2}\right] \quad \text{Eq. 1}$$

Where Pe represents the permeability of the membrane, δ denotes the thickness of the membrane, $p_{H_{2,ret}}$ and $p_{H_{2,perm}}$ represent the hydrogen partial pressure on the retentate and permeate sides, respectively, and n represents the exponential factor that indicates the rate-limiting step of the mechanism by which hydrogen crosses the selective palladium layer. In the case of ideal conditions where there is thermodynamic equilibrium between the hydrogen atoms dissolved at the membrane surface and the hydrogen concentration in the gas phase, the pressure exponent n is equal to 0.5. In this scenario, Richardson equation (Eq. (1)) takes the form of Sieverts' law (n = 0.5), suggesting that the diffusion of hydrogen

atoms through the bulk of Pd is the limiting step in the hydrogen permeation mechanism. The membrane permeability Pe can be expressed using an Arrhenius-type correlation, as described in Eq. (2).

$$Pe = Pe_{0,H_2} e^{-\frac{E_a}{RT}} \quad \text{Eq. 2}$$

where Pe_{0,H_2} represents the pre-exponential factor, E_a is the activation energy, R denotes the universal gas constant, and T represents the temperature. The permeation parameters utilized in the study are sourced from the literature, specifically the experiments conducted by Fernandez et al. (2015) [52], which closely align with parameters obtained from similar membranes [53,54] as presented in Table 2.

When describing hydrogen extraction from a mixture through a highly selective and permeable membrane, experimental findings indicate that Sieverts' law alone is insufficient [55,56] for predicting the transmembrane flux due to a phenomenon known as 'concentration polarization' (CP). To accurately describe the membrane permeation it is necessary to determine the concentration at the membrane surface [57,58]. In this work this phenomena is integrated into a so called 'CP factor' which is used as a multiplier in Sieverts' law. A CP factor of 0.15, determined through Computational Fluid Dynamics (CFD) simulation, is applied [59]. However, other research suggests the potential for a higher contribution from concentration polarization [55]. Due to the very high selectivity of dense membranes, in the model it is assumed that only hydrogen crosses the membranes (so an infinite ideal selectivity), and then the permeate side is pure hydrogen. The effect of membrane ceramic support is neglected. Finally, accurately accounting for reaction kinetics is essential in modeling catalytic reactors as it can significantly impact equipment size and cost [47]. NH_3 decomposition into H_2 and N_2 occurs according to the following midly endothermic reaction (cf. Eq. (3)) which and is therefore thermodynamically favored at high temperatures. Moreover, according to the Le Châtelier's principle, as ammonia decomposition occurs with molar expansion, it is favored at low pressure.

$$NH_3 \leftrightarrow \frac{1}{2}N_2 + \frac{3}{3}H_2 \Delta H_f^{\circ} = 45.9 \frac{kJ}{mol} \quad \text{Eq. 3}$$

For numerical simulation, a mathematical representation of the ammonia decomposition reaction rate is essential. Several studies have used Temkin-Pyzhev-like power laws, as described in Eq. (4) to match the experimental conversion [60,61]. This model, while relatively straightforward, has been found to predict empirical data by fitting the reaction order β, Activation energy E_{act}, and the pre-exponential factor k_0. The assumptions made in the membrane reactor model are detailed in Table 3. Additional information on kinetic models and sensitivity analyses is available in Supplementary Materials S.4 and S.5.

$$R_{NH_3} = k_0 e^{-E_0/RT} \left(\frac{{p_{NH_3}}^2}{{p_{H_2}}^3} \right)^{\beta} \quad \text{Eq. 4}$$

2.3. Techno-economic model

A preliminary techno economic assessment is conducted to compare the different plants on the hydrogen production island and at the power plant level. Following recommended methodology adopted in the literature [62–65], the total plant cost (TPC) is calculated as per Eq. (5)

Table 2
Fitted parameter in the Sievert law of the most common Pd 0.85 Ag 0.25 on ceramic support (up to 3.5 mm). and fitted parameter in the Sieverts law.

Reference	Thickness [μm]	Pre exponential factor $[mol\, m^{-1} s^{-1} Pa^{-0.5}]$	E_{act} [kJ/mol]
[54]	4.2	$1.76 * 10^{-8}$	7.1
[53]	5.2	$4.57 * 10^{-8}$	9.23
[52]	5	$6.93 * 10^{8}$	9.99

Table 3
Membrane reactor specifications.

Parameters	Unit	Value
Membrane OD	*m*	0.014
Membrane Length	*m*	2.7
Reactor diameter	m	0.7
Active height of the bed	m	3
Number of membranes per reactor	–	260
Membrane volumetric coverage	[−]	0.1
Start position of the membrane	*m*	0.3
Catalyst density	kg/m^3	980
Bed porosity β	–	0.4
CP Factor	–	0.15

with a bottom-up approach breaking down the power plant into the basic components or equipment, and then adding installation costs (TIC), indirect costs (IC) and owner's and contingencies costs (C&OC).

$$TPC = \left(\sum_i C_i \right) * (1 + \%_{TIC}) * (1 + \%_{IC}) * (1 + \%_{c\&OC}) \quad \text{Eq. 5}$$

The costs associated with the hydrogen production island were determined using correlations adapted from Turton et al. (2018) [66] for stainless steel material, which was selected due to the corrosive nature of ammonia. The component costs for the power island were derived from literature sources as presented in Table 4 and scaled using Eq. (6), where the reference size is denoted as $S_{i,0}$ and the reference cost is denoted as $C_{i,0}$.

$$C_i = C_{i,0} \left(\frac{S_i}{S_{i,0}} \right)^f \quad \text{Eq. 6}$$

The purchased cost derived from these correlations for the power island closely matches that obtained from a separate Thermoflow™ analysis with only an 8% difference observed. This consistency reinforces the validity and appropriateness of the chosen correlations. The component prices are then updated using the Chemical Engineering Plant Cost Index (CEPCI) method for considering price fluctuations like inflation, deflation. For this analysis, an index of 701 was used to adjust to the 2021 period.

The TPC is converted in an annualized operating cost using the Capital Charge Factor (CCF) as described in Eq. (7) as a function of the discount rate *i* and the plant lifetime *n*.

$$CCF = \sum_{j=1}^{N} \frac{1}{(1+i)^j} = \frac{i \times (1+i)^n}{(1+i)^n - 1} \quad \text{Eq. 7}$$

Subsequently, the final cost of hydrogen (LCOH) and cost of electricity (LCOE) were estimated following the acknowledge formula

Table 4
List of assumptions cost assumption for plant component cost calculated using a scaling law method [67].

Equipments	Scaling parameter	Ref capacity S_0	Ref erected cost C_0	Scale factor f	Cost year
Gas turbine, generator and auxiliaries.	Power net [MW]	272.12	49.4	0.3	2007
HRSG, ducting and stack.	U·S [MW/K]	12.9	32.6	0.67	2007
Steam turbine, generator and auxiliaries.	Power gross [MW]	200.0	33.7	0.67	2007
Cooling water system and BOP.	Heat rejected [MW]	470.0	49.6	0.67	2007
MEA CO_2 separation system.	CO2 captured [kg/s]	38.4	29.0	0.8	2007

defined in Eq. (8) and Eq. (9). These two metrics are composed of the annualized *TPC* and the Operations and Maintenance fixed $C_{O\&M.fix}$, and variables $C_{O\&M.var}$ those two costs are represented by consumables (e.g. catalyst, reactant, water and membranes) and auxiliaries, maintenance, insurance and operators cost) divided by the plant productivity (viz. hydrogen or electricity production).

$$LCOH\left[\frac{€}{Nm^3}\right] = \frac{(TPC[€] \times CCF[\%/year]) + C_{O\&M.fix}[€/\text{year}] + \left(C_{O\&M.var}\left[\frac{€}{year}\right] \times h_{eq}\right)}{Production\ capacity\left[\frac{kg}{year}\right] \times h_{eq}\left[\frac{h}{year}\right]} \quad \text{Eq. 8}$$

$$LCOE\left[\frac{€}{MWh}\right] = \frac{(TPC[€] * CCF[\%/year]) + C_{O\&M.fix}[€/\text{year}] + \left(C_{O\&M.var}\left[\frac{€}{year}\right] \times h_{eq}\right)}{Production\ capacity\left[\frac{MWh}{year}\right] \times h_{eq}\left[\frac{h}{year}\right]} \quad \text{Eq. 9}$$

Economic estimations are inherently subjected to a wide range of uncertainties as detailed by Neveux et al. (2020) [68]. In this study three main sources of uncertainties are considered, associated namely to the type of estimation being performed, to the technological maturity of the process considered, (i.e., the level of understanding of the process) and lastly to the price of ammonia. The first two have a ripple effect on the production cost of the process This is because they influence the key elements involved in computing production costs, particularly CAPEX and in a lesser extent the OPEX, which are proportional to the various terms of the installation investment. A Monte Carlo sampling technique performing 10,000 simulations per technology system is employed to propagate uncertainties in production costs. A log-normal distribution is used to represent each uncertainty distribution [68].

The uncertainties related to technology and preparation effort are already quantified by the AACE (Association for the Advancement of Cost Engineering) [68,69]. Concerning technological uncertainty, the Furnace Technology Reforming (FTR) has a higher Technology Readiness Level (TRL) than the Membrane Reactor (MR). This is primarily because several commercial electric-based furnaces, albeit on a smaller scale, already exist and could potentially be upscaled. It is also worth mentioning that for example Topsoe have commercial offer of cracking unit as big as 500 ton per day of H_2 [70]. Furthermore, the FTR technology closely aligns with conventional natural gas reforming systems, which currently account for over 95% of the world's hydrogen production at scales exceeding 50,000 Nm^3/hr [71]. The proven experience and successful implementation of this technology indicate a swift increase in TRL. Therefore, the ammonia FTR technology is assigned a virtual TRL of 7. On the contrary, membrane reactors currently stand at TRL 4–5. However, the ongoing European Project Arenha [72] is dedicated to advancing this technology to TRL 6, signaling progress in its development and bringing it closer to commercial readiness. Fig. 4 illustrates how both uncertainties are incorporated into the TPC calculation, including the addition of installation costs, indirect costs, and the costs for owner's contingencies taken in adequation with literature.

When considering feedstock uncertainty, current forecasts, based on existing technology and an average renewable electricity cost of 44 €/MWh [73], suggest that green ammonia would cost at least 578 €/ton in 2019. Nevertheless, with the continuous evolution of Power-to-Ammonia processes, substantial advancements are expected in

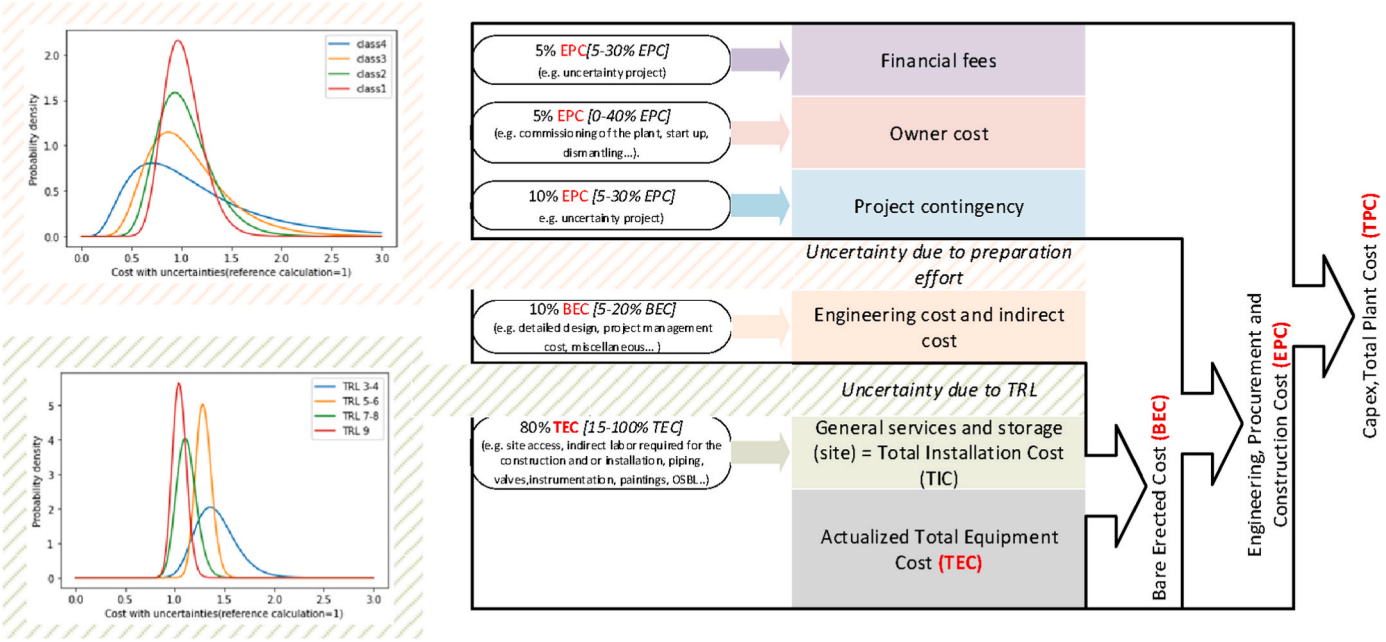

Fig. 4. Determination of the TPC through a bottom up approach and uncertainty propagation on the TRL and Preparation effort as recommended by Neveux et al. (2020) [68].

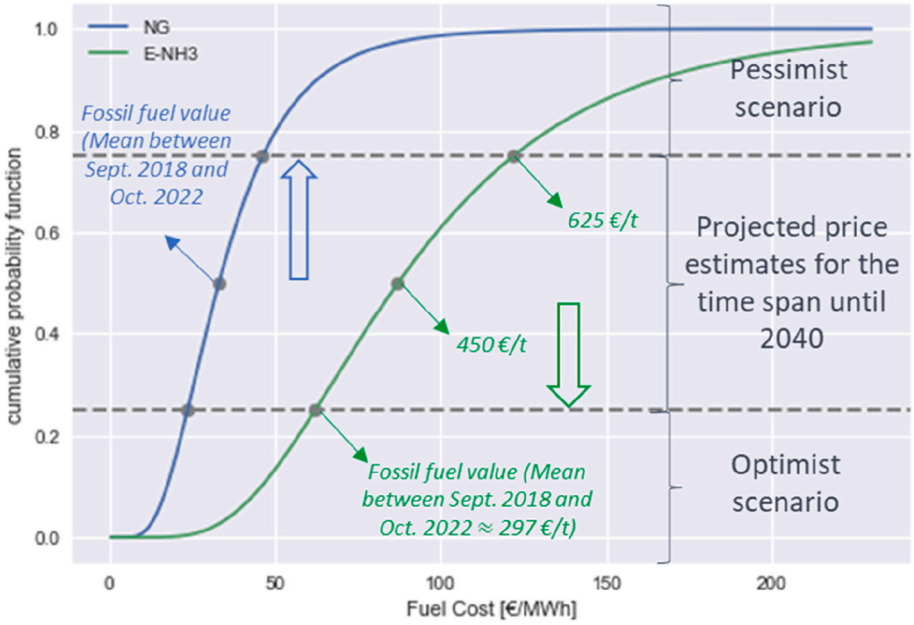

Fig. 5. Cumulative fuel cost distribution for Natural Gas and E-NH_3: Future price projections trends are Illustrated by Arrows. (Optimistic scenario below 1st quartile, signifying potential for competitive costs with green ammonia or natural gas & Pessimistic scenario above 2nd Quartile). (For interpretation of the references to colour in this figure legend, the reader is referred to the Web version of this article.)

Table 5
Main assumptions related to the techno-economic analysis.

O&M Fixed Cost	Cost (€)
Maintenance cost	0.025*TPC [64]
Insurance	0.02*TPC [64]
Labor cost (no retrofit)	6 M€ [64]
Labor cost (retrofit)	9 M€ [64]
O&M Variable	Cost (€)
Ammonia cost (€/kg)	450 €/ton
Ammonia storage cost (€/kg)	0.9 [84]
NG cost	9.15 €/GJ_{LHV}
Water cost	6€/m^3 [85]
Pd Membrane cost	6000 €/m^2
Electricity cost	60 €/MWh
Catalyst cost	143 €/kg
Membrane lifetime	3 years
Membrane cost recovery	0.5*Membrane Cost
Catalyst lifetime	5 years
Carbon tax (for NG CCGT)	25 €/t_{CO2}
General Assumptions	
Discount rate CCF	0.153
Plant Capacity factor	0.65
CEPCI	701 (2021 period)

the coming years. Projections indicate that by 2040, green ammonia could compete with fossil-based ammonia, with an estimated cost range of 210–215 €/ton if electricity prices fall below 20 €/MWh [49]. According to Fasihi et al. (2021) [74], estimated prices for renewable ammonia in 2030 range between 370 and 450 €/ton, and in 2050, between 285 and 350 €/ton. Cesaro et al. (2021) [49] estimated around 345 €/ton for ammonia by 2040. The literature provides a wide range of prices for renewable ammonia fuel, spanning from 210 to 1224 $/ton [75–77], highlighting the potential for lower prices to emerge by the 2040–2050 timeframe. Fig. 5 depicts a probability distribution outlining different scenarios. Values below the 25th percentile in the distribution signify an optimistic scenario where prices would be below the current market rate. Similarly, the price of natural gas is subject to significant fluctuations influenced by various factors, including supply and demand dynamics, geopolitical tensions, and environmental regulations. Recent trends indicate an increase in volatility within natural gas prices, and this volatility is expected to intensify in the future. The median value represents the average ammonia natural gas price observed during the current period (September 2018 to October 2022).

Table 5 presents the key assumptions utilized for estimating the levelized costs in the base case scenario these assumptions are less prohibitive than the other therefore no uncertainty is propagated. Some of these assumptions are briefly discussed below. In the literature, catalyst costs often vary widely, typically calculated based on material cost per weight, leading to substantial discrepancies. For instance, Yoshida et al. (2021) [78] estimated the cost of Ru/C catalyst at around 295 €/kg, while Makhloufi et al. (2021) [47] used a cost of 22.3 €/kg and concluded that the impact of this factor on the final cost was negligible. To arrive at a compromise, this study adopts a catalyst cost of 143 €/kg [79] and assumes a lifespan of 5 years. The cost of membranes, including the recycling of both Pd–Ag waste and membranes can be estimated to range from 2000 to 5000 €/m^2 [80], according to the FluidCell Eu. Project [81]. The membrane lifetime for Pd–Ag membranes at temperatures $\leq$425 °C was previously estimated to be 3 years, but it is expected to increase to 5 years, as targeted by the Macbeth Eu. Project [82]. The baseline scenario for this study assumes a membrane cost of 6000 euro/m^2 [83], with a recovery factor of 0.8 considered to account for the recycling process. Another crucial assumption pertains to the capacity factor, where it is presumed that the plant operates at full load for a portion of the time and is inactive for the remainder, even though real-world plants often operate at partial load for certain periods. The assumed capacity factor in this context is 0.65. A carbon tax is also imposed on the natural gas combined cycle gas turbine (NG CCGT). Examining European countries with an implemented carbon tax reveals a range of values, from 116 €/ton $_{CO2}$ in Sweden to as low as 0.07 €/ton$_{CO2}$ in Poland. For the purposes of this study, a carbon tax of 25 €/ton $_{CO2}$ is applied.

2.4. Performance indicators

Beyond economic indicators, several metrics are used to evaluate and contrast the performance of the reactors under diverse operating conditions. Two such metric are the ammonia conversion X_{NH_3} and the hydrogen recovery factors HRF_{NH_3} as defined in Eq. (10) and Eq. (11)

The latter pertains to the overall amount of pure H_2 separated by the membrane, relative to the total H_2 fed into the reactor (based on the stoichiometry of the reaction).

$$X_{NH_3} = \frac{F^{Ret}_{NH_3,in} - F^{Ret}_{NH_3,out}}{F^{Ret}_{NH_3,in}} \quad \text{Eq. 10}$$

$$HRF_{NH_3} = \frac{F^{Per}_{H_2,out}}{\frac{3}{2}F^{Ret}_{NH_3,in}} * 100 \quad \text{Eq. 11}$$

These metrics anyhow do not consider heat integration and auxiliaries' consumption of the overall plant. At the fuel processor level, an intermediate hydrogen thermal efficiency denoted (η_{th}) is defined in Eq. (12) as the ratio of the energy output associated to the produced hydrogen by the total thermal input power discounting the electricity consumption.

$$\eta_{th} = \frac{F_{H_2} LHV_{H_2} - W_{aux}}{F_{NH3}\, LHV_{NH_3}} \quad \text{Eq. 12}$$

W_{aux} is the sum of the electric consumptions of the system auxiliaries (i.e. compressors, pumps, control system) and $LHV_{H_2} = 120\ MJ/kg$ and $LHV_{NH_3} = 18\ MJ/kg$.

3. Results and discussion

This section starts with the validation of the reactor model and a discussion on existing catalyst performance. It is then followed by a sensitivity analysis that contrasts the Membrane Reactor (MR) with the Traditional Reactor (TR) at the reactor level before extending the comparison to the hydrogen production and CCGT levels, using a natural gas-fed plant as a reference.

3.1. Reactor model validation

The modeling of catalytic reactors is heavily reliant on the accurate consideration of reaction kinetics, which can have a substantial impact on equipment size and cost. The kinetic law parameters (from Eq. (4)) were fitted for several Ruthenium (Ru)-based catalysts cited in the literature Hypermec 10010™ (8% Ru) [60] and Alfa Aesar™ (2% Ru) [41] and a non-commercial catalyst based on Ru (3%)-K-CaO [86]. A nickel-based catalyst was also considered for reference [87]. For the interested reader, details are presented in Supplementary Material S4. Fig. 6 offers a direct comparison of reactant conversion for the mentioned catalyst under similar conditions ($P_{ret} = 10$ bar, $W/F = 2$ kg h kmol^{-1}). Additionally, for the Ru (3%)-K-CaO catalyst, a membrane is integrated with assumed values of $P_{perm} = 0.1$ bar and two different CP factors 0.2 and 0.5. This graph clearly illustrates that a higher loading of Ru results in greater conversion at a given temperature. Moreover, it shows that when the Ru (3%)-Ru-K-CaO catalyst is used as a membrane reactor (indicated as MR in the graph), it surpasses the performance of more heavily loaded catalysts under those conditions. Across the studied temperature range, this catalyst achieves an average conversion rate five times higher than the standard, less costly nickel-based catalyst. However, to attain complete conversion using this catalyst, extremely high temperatures (above 700 °C) are necessary.

3.2. Sensitivity study at the reactor level

In this section, a sensitivity analysis is carried out comparing the performance of MR and TR reactors at the reactor level. Using the catalyst from Sayas et al. (2020) [88], which has been validated at higher pressures, the impact of Gas Hourly Spaced Velocity (GHSV) is explored at T = 425 °C $P_{ret} = 10$ bar for the TR and considering $P_{perm} = 0.1$ bar and a CP factor of 0.25 for the MR. Fig. 7 a shows that the ammonia conversion in the MR reach up to 87% higher conversion than the TR at GHSV = 500 hr^{-1} and the gap reduced progressively with 15% at 4000 hr^{-1}. Additionally, a swap point becomes apparent, where the membrane reactor transitions from a regime in which it produces more hydrogen than the TR at low space velocities to the opposite scenario. Fig. 7 b provides further insights into this situation. Firstly, it shows that HRF follows a similar trend as conversion, decreasing as GHSV increases. On the other hand, the recovered hydrogen flow rate, is found to increase with GHSV up to a maximum value at around 1000 hr^{-1}, then decreases as GHSV continues to rise. This observed trend is consistent with findings from other studies in the literature, such as Sitar et al. (2022) [89], who also found that as temperature increases, the point of

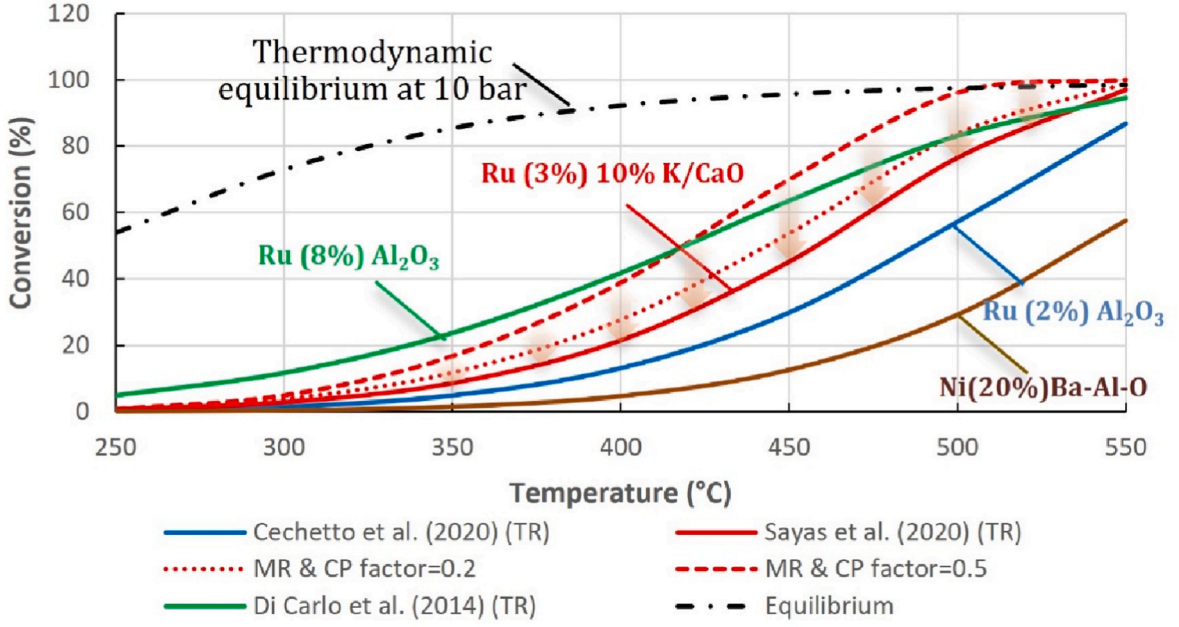

Fig. 6. *Conversion vs Temperature obtained for four catalysts. The conversion obtained with TR are represented by continuous line. The conversions obtained with MR for Sayas et al. (2020) [86]'s catalyst are represented with a dashed line considering two different concentration polarization reducing factors namely 0.2 and 0.5 (P=10 bar, T=250–550 °C, W/F = 2 kg h kmol^{-1}, P_{perm}= 0.1 bar).*

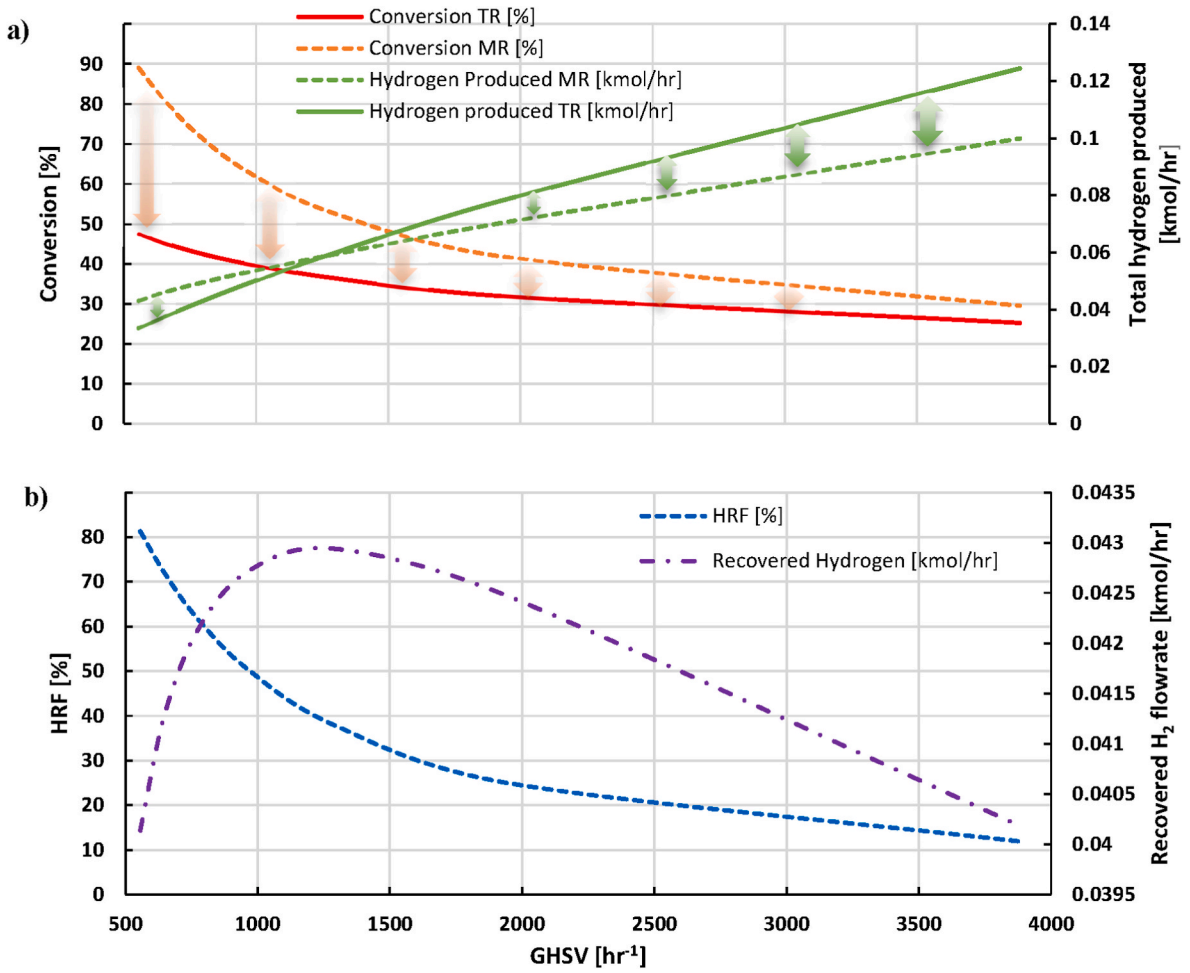

Fig. 7. Effect of GHSV on the ammonia decomposition equipped Ru (3%) K–CaO catalyst [86] (T = 425 °C, P_{ret} = 10 bar P_{perm} = 0.1 bar) a) Conversion and Total hydrogen production for both TR and MR b) HRF and Recovered hydrogen for the MR.

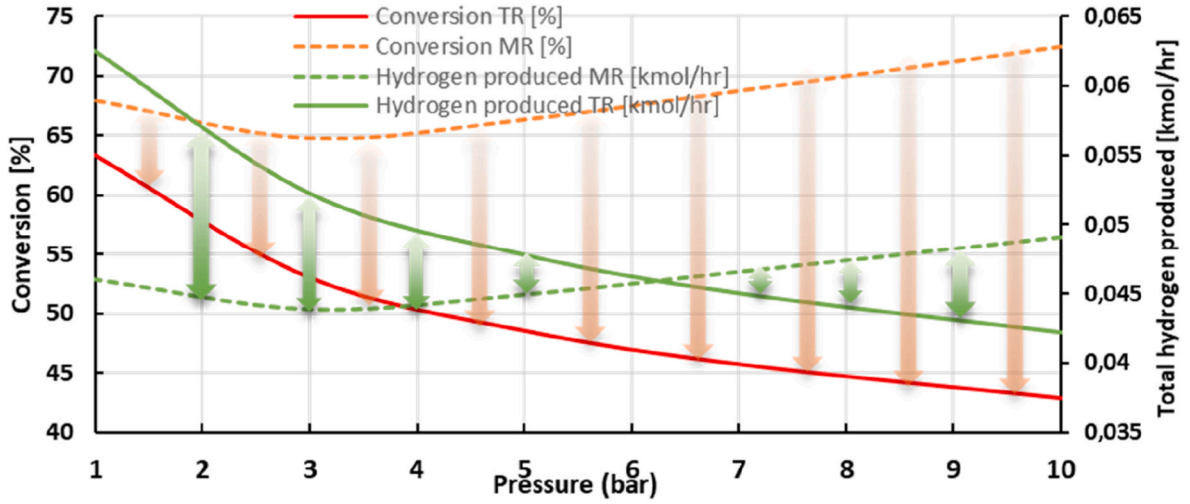

Fig. 8. Effect of reaction pressure on the ammonia decomposition Conversion and Total hydrogen production for both TR and MR (T = 425 °C, P_{perm} = 0.1 bar, W/F = 5).

maximum recovery shifts towards higher GHSV values. Chen et al. (2023) [90] revealed a similar location as our study reaching a maximum recovered hydrogen flow at GHSV = 1100 h^{-1} at T = 400 °C. Finally, Cerrillo et al. (2021) [45] obtained also a similar maximum between 1260 and 1860 mL/g_{cat}/hr which correspond to the space velocity range observed in this study. Clearly, membrane reactors demonstrate improved performance within a particular space velocity range when assessed on reactor-level criteria. When space velocities are high, the membrane faces challenges in permeating the produced hydrogen, which results in reduced H_2 recovery. It appears

advantageous to operate at lower space velocities. Yet, it is important to highlight that this represents just one of many considerations. For instance, increasing the ammonia feed rate leads to a higher hydrogen purity in the emitted gas [40]. An additional sensitivity study examines the effect of pressure, as shown in Fig. 8. The retentate side pressure is varied from 1 bar to 10 bar, while the permeate side pressure is maintained at 0.1 bar, and the W/F ratio is set to 5 kg h $kmol^{-1}$. As often observed [59,90], a pressurized feed benefits H_2 production in a membrane reactor, but it has a negative impact on the ammonia decomposition in the catalytic reaction. The increase in conversion is found notably 70% higher at 10 bar and 36% higher at 5 bar than the TR reactor. It is important to note that a pressure of at least 5–6 bar seems to be required for the MR to outperform the TR. This illustrates that the design of membrane reactors involves several conflicting trade-offs to consider.

3.3. Ammonia cracking system analysis

The economic purpose is clearly to identify the operating conditions and reactor geometries which minimize the LCOH. In order to detail the performance of the MR system, sensitivity studies are performed at designated ammonia flow rates while adjusting the number of reactors, thereby altering the Gas Hourly Space Velocity (GHSV), to maintain the necessary hydrogen production. The outcomes of this study are presented in Fig. 9 (a) and Fig. 9 (b):Fig. 9 (a) displays the cumulative effect of pressure and number of reactors (and therefore GHSV), while Fig. 9 (b) illustrates the impact of temperature and GHSV on both thermal efficiency and cost.

When considering the effect of pressure (cf. Fig. 9 (a)) on the LCOH, it is generally observed that higher pressures have a positive impact. In general, higher pressures allows to reach the minimum at a lower number of membranes, which is preferred since membranes are a breakable component in the reactor. However, as the pressure is raised to even higher levels, its effect on the LCOH becomes less significant. On average, the most significant relative change in LCOH is observed when the pressure is raised from 10 to 15 bar, resulting in a mean LCOH reduction of almost 7%. In contrast, the LCOH only decreases by 2% when the pressure is raised to 20 and 25 bar. This observation can be put in relation with the number of reactors required which decrease by 25% between 10 and 15 bar and by 12% between 20 and 25 bar. While higher pressures privilege hydrogen permeation through the membrane, they do not favor the cracking reaction. Upon observing the thermal efficiency, it becomes evident that the influence of pressure is rather limited, leading to only a slight improvement in efficiency. This can be attributed to the reduction in reactor size and GHSV per reactor, which results in excess heat in the burner exhaust beyond what's needed for reactant pre-heating.

Regarding the effect of temperature (cf. Fig. 9 (b)) ammonia decomposition is an endothermic process, so the conversion of ammonia into hydrogen and nitrogen is enhanced at elevated temperatures. However, temperatures above 500 °C can compromise Pd-based membrane stability, hence it is advisable to avoid such conditions [91]. Analysis within this study showed raising the temperature from 400 °C to 460 °C decreased the LCOH by 4.8% and reduced the number of reactors by 30%, with the most significant reductions and cost savings occurring between 400 °C and 430 °C.

Table 6
Summary of optimized conditions of the MR subjected to the following constraints H_2 productivity of 2600 kmol/h at 30 bar.

	Objective	Maximized Efficiency	**Minimized LCOH**	Minimized Number of reactors
Parameters	NH_3 flowrate [kmol hr^{-1}] ϵ [1700–2700]	2067	2046	1922
	Reactor inlet pressure [bar] ϵ [10–20]	20	20	20
	Reactor temperature [°C] ϵ [400–460]	440.6	439.4	442
	Number of reactors [−] ϵ [55–120]	66.3	57.05	55
Results	GHSV [hr^{-1}]	585	570	653
	Thermal efficiency [−]	0.84	0.85	0.81
	LCOH [€/kg_{H2}]	4.48	4.45	4.47
	NOX emissions from the cracking step [kg_{NOX}/kg_{H2}]	0.021	0.018	0.036

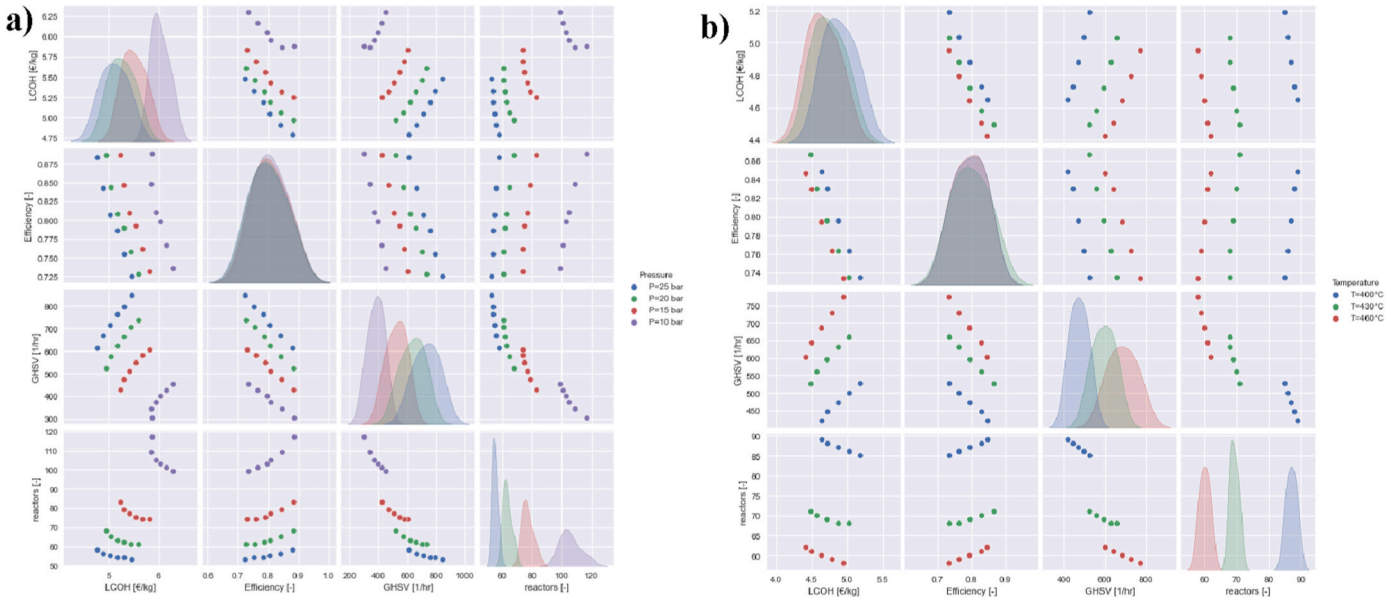

Fig. 9. a) Sensitivity study on the effect of pressure & GHSV on the thermal efficiency and LCOH b) effect of reactor temperature on the LCOH. In this investigation the delivery pressure of hydrogen is assumed to be 30 bar.

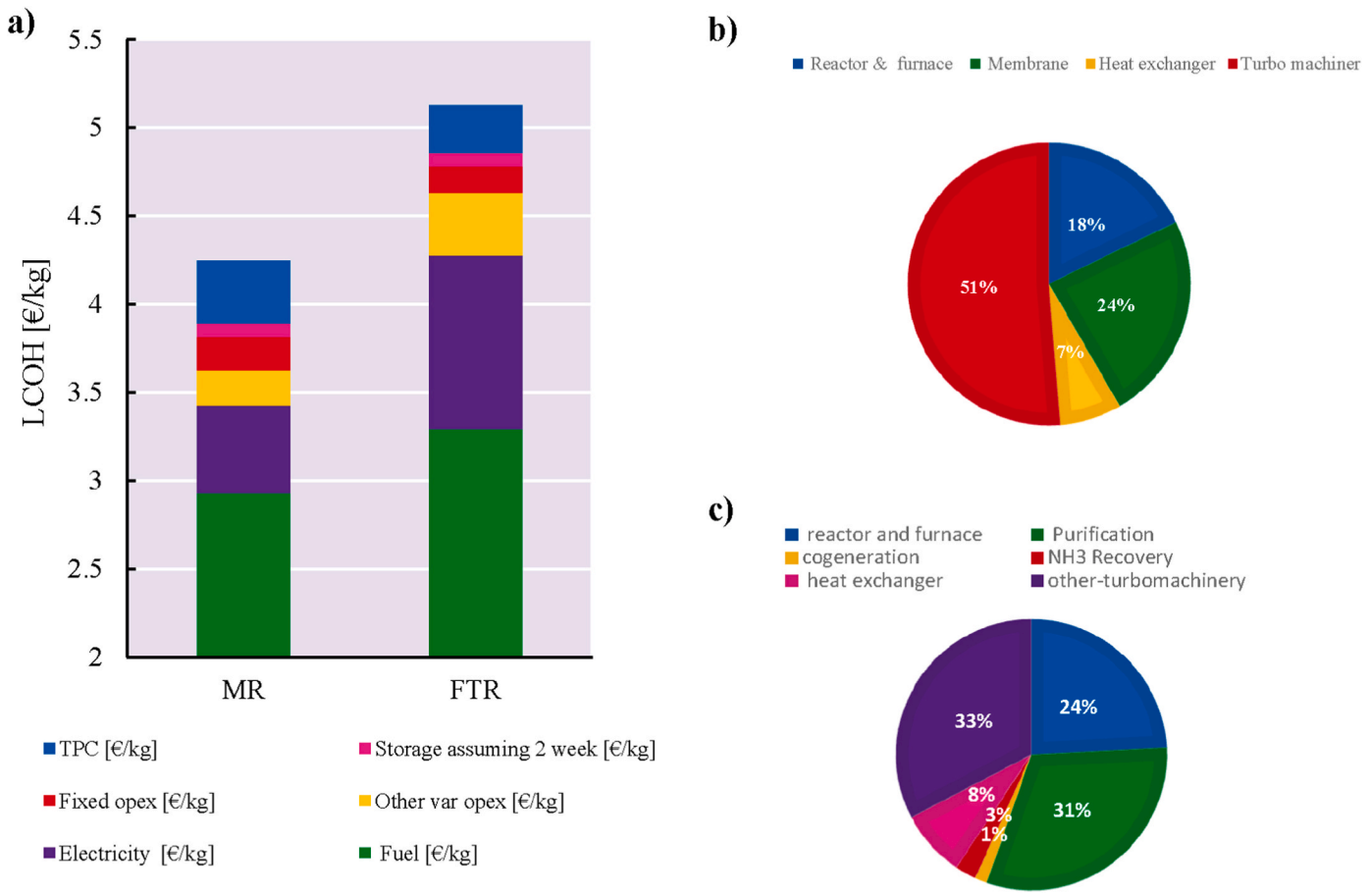

Fig. 10. LCOH cost breakdown and TPC composition for the MR and FTR systems a) LCOH cost breakdown, b) TPC composition MR system and c) TPC composition FTR system at the same hydrogen delivery pressure of 30 bar.

Finally, to optimize the flowsheet structure's parameters conveniently, such as permeate pressure, reactor inlet pressure, flow rate, temperature, and the required number of reactors, the SQRP (Sequential Quadratic Programming) feature of Aspen Plus software is employed. This method proves highly beneficial to help select the appropriate design and operational parameters when the architecture is established. Results for the best design case are reported in Table 6 together with the optimized parameters. The economic optimum appears to deviate slightly from the efficiency and membrane optima. However, considering the precision of equipment cost correlations, it is plausible to

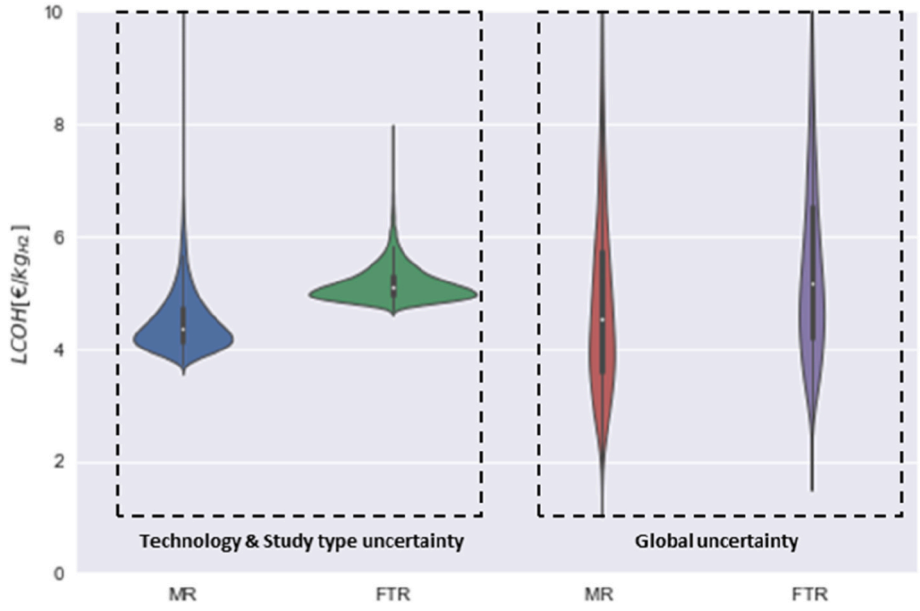

Fig. 11. LCOH distribution comparing the technology uncertainty to the global uncertainty.

suggest that these optima may be somewhat conflated within the context of this process architecture.

As reported in Fig. 10, the MR system outperforms the reference FTR system, with a 30% increase in thermal efficiency and a 10% drop in the Levelized Cost of Hydrogen (LCOH) to 4.45 €/kg-$_{H2}$. Meanwhile, the FTR system achieves a 68.5% thermal efficiency with an LCOH of 5.1 €/kg-$_{H2}$, marginally above findings by Makhloufi et al. (2021) [47]. The discrepancy is partly due to the FTR's lower productivity in this study, about two-thirds of the original work. These LCOH figures are considerably above the Steam Methane Reforming (SMR) costs of 1.70 $/kg-$_{H2}$ to 2.09 $/kg-$_{H2}$, largely due to the assumption of ammonia spot prices [92].

The cost breakdown shows the LCOH is largely driven by green ammonia prices, contributing to 70% of the MR system's LCOH and 65% of the FTR's. Due to its greater efficiency, the MR system uses less fuel and incurs lower operating expenses compared to the FTR system, yet it has the highest Total Purchased Equipment Cost (TPC). Significantly, 85% of the FTR system's TPC is allocated to cracking, purification, and compression. In addition, the results can be presented using violin plots, which provide a comprehensive visualization of statistical data, including the probability density of each system based on the technology and type of estimation, as well as the uncertainty in feedstock prices. Fig. 11, emphasizes the significant impact of fuel cost on the LCOH, highlighting its key sensitivity in relation to technology and study type uncertainty. Additionally, further sensitivity studies not included in the uncertainty analysis can be found in the Supplementary Material S.5.

3.4. Techno economic comparison at the CCGT level

In this section, the comparison extends to the level of the Combined Cycle Gas Turbine. Fig. 12 a showcases the LCOE while considering uncertainties related to technology and preparation effort for both the retrofit solutions and the conventional natural gas Combined Cycle Gas Turbine. Fig. 12 b represents the global effect of the uncertainties on the

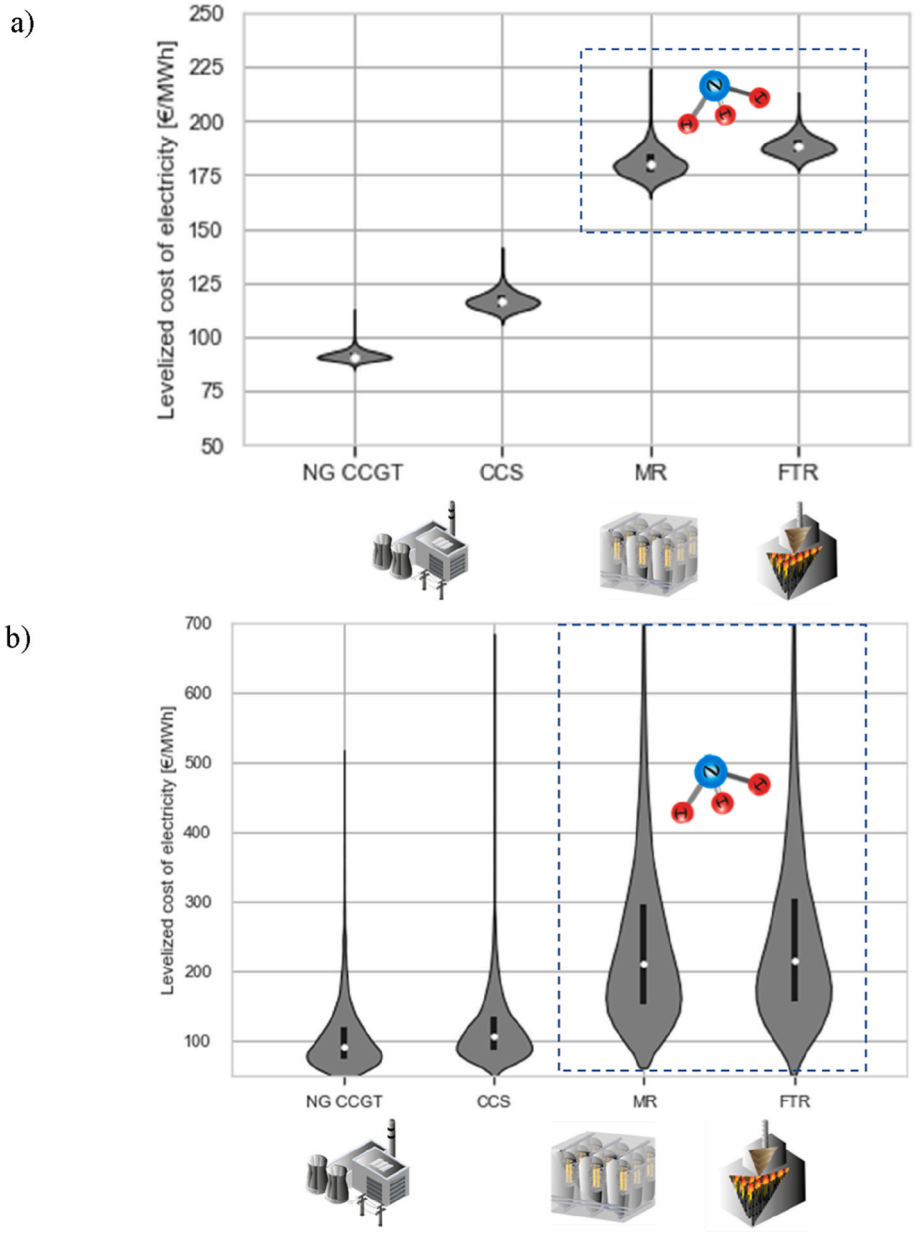

Fig. 12. LCOE comparison using 65% power plant capacity factor a) Technology and preparation effort uncertainties and b) Total uncertainty (a carbon tax of 25 €/ton is assumed for the NG CCGT).

LCOE for each technology. At the median, ammonia contributes to approximately 80% of the Levelized Cost of Electricity, while natural gas accounts for around 60%. This indicates that ammonia has a significant impact on the overall LCOE. Therefore, variations in fuel prices can have a substantial influence on the LCOE, making it a critical factor to consider in cost analyses. When considering CAPEX, the FTR and CCS technologies demonstrate similar magnitudes, with values of around 20.6 €/MWh and 19.4 €/MWh, respectively. On the other hand, the membrane reactor (MR) has a slightly higher CAPEX, reaching approximately 26 €/MWh. In terms of the CAPEX share in the LCOE, this study finds that in the baseline scenario, the CCS technology accounts for 20% of the LCOE, while the FTR and MR technologies contribute 5% and 8%, respectively. This emphasizes the fact that fuel cost constitutes the major portion of the LCOE for these two technologies, overshadowing the influence of CAPEX on the overall cost. Therefore, when focusing on the lower range of fuel prices (below the lower quartile) that are more in line with projected prices for 2040–2050, the ammonia blend could be competitive with the reference NG CCGT under certain conditions. This finding aligns with the conclusions of Cesaro et al. (2021) [49]. Finally, besides considering the levelized cost of electricity, insights can be derived from the research conducted by Helmi et al. (2015) [93]. Their study investigates the required amount of palladium for a membrane reactor in an integrated gasification combined cycle unit for carbon capture. This study indicates that retrofitting the equivalent of 1 GWe facility would need approximately 10% of the global annual ruthenium production and around 0.11% of the global annual palladium production as detailed in Table 7 and Table 8. Thus, it's crucial to recognize the challenge posed by the scarcity of materials in adopting this technology. The constrained supply of these materials, coupled with their extensive demand for achieving net-zero goals and the possible implications of geopolitical tensions - particularly given the concentration of production in South Africa and Russia [94]- renders this approach impractical. This is especially true when considering that as of 2021, approximately 1.8 TW of natural gas turbines have already been installed worldwide [92]. Supplementary Material S.7 provides details on the supply, demand, and recent price fluctuations of ruthenium and palladium. To tap into this market, future research should prioritize the exploration of alternative membrane materials, such as carbon molecular sieve, and catalysts, like nickel.

Table 7
Detail of the calculation to the mass of palladium required to retrofit 1GWe of CCGT asset (total palladium supply in 2022:210 tons) [94].

Membrane length [m]	2.7
Membrane diameter [m]	0.014
Number of membranes [−]	210
Number of reactors [−]	64
Density of palladium [kg/m^3]	12000
Surface area of membrane per reactor [m^2]	24.93
Volume of palladium per reactor [m^3]	0.00012
Mass of palladium per reactor [kg]	1.49
Mass of palladium per reactor kg for 1 CCGT plant ~ 400 MW [kg]	97.2
Mass of palladium for 1GWe [kg]	243.1
World Ruthenium production in 2022 [kg]	210000 [94]
As a percentage of the world palladium production [%]	~0.11%

Table 8
Detail of the calculation to the mass of Ruthenium required to retrofit 1GWe of CCGT asset.
(the Global ruthenium production, generally not disclosed, is estimated at 27.8 tons [95]).

Active volume of the bed (1 reactor) [m^3]	1.06
Catalyst type	Sayas et al. (2020) [88]
Bed density calculated [kg/m^3]	846
Number of reactors [−]	65
Mass of ruthenium per reactor [kg]	18.1
Mass of palladium per reactor kg for 1 CCGT plant ~ 400 MW [kg]	1174.4
Mass of ruthenium for 1GWe [kg]	2936.1
World Ruthenium production in 2020 [kg]	27800 [95]
As a percentage of the world Ruthenium production [%]	~10%

4. Conclusions

Incorporating ammonia into existing combined cycle gas turbine (CCGT) assets through co-firing with hydrogen in a specific blend holds promise as a viable strategy. However, the primary hurdle lies in advancing the development of efficient technology for ammonia cracking. To address this, the present study conducted a preliminary techno-economic assessment of two cracking technologies taking into account uncertainties in feedstock costs, technology maturities, and preparation efforts for both cracking and CCGT. Special emphasis was placed on the detailed design of the membrane reactor plant.

At the reactor level, a sensitivity study delved into the effects of various catalysts and operating conditions for both membrane and traditional reactors. Notably, increasing the Gas Hourly Space Velocity (GHSV) led to decreased ammonia conversion and H_2 recovery, pinpointing an optimal GHSV that maximizes H_2 recovery. From the hydrogen production criteria the membrane reactor emerges as a better system only in a very limited space velocity range.

At the hydrogen production plant level, through various optimizations, the membrane reactor system demonstrated superior performance compared to the reference FTR (Fired Tubular Reactor) system. It exhibits a 30% increase in thermal efficiency and a 10% reduction in the levelized cost of hydrogen (LCOH), resulting in a LCOH of 4.45 €/kg$_{H2}$. On the other hand, the FTR system operates at a thermal efficiency of 68.5% and achieves a LCOH of 5.1 €/kg$_{H2}$. While the MR system benefits from a decreased fuel expense, its capital expenditure (CAPEX) is notably higher than that of the reference system. It is essential to reminds that these results were derived based on specific process architectures and at a particular scale of hydrogen production.

At the CCGT level, the difference in levelized cost of electricity (LCOE) becomes less pronounced, given the heavy influence of ammonia costs, which contribute to 80% of the LCOE. Beyond LCOE, material scarcity poses another hurdle for these systems' wider adoption. For instance, retrofitting just 1 GWe of CCGT assets with membrane reactors would demand about 0.11% of the global palladium and 10% of the global ruthenium production. Given these challenges, it is evident that exploring alternative materials is vital to truly harness the potential of retrofitting existing assets with ammonia-hydrogen blends.

CRediT authorship contribution statement

Simon Richard: Writing – original draft, Investigation, Data curation, Conceptualization. **Alvaro Ramirez Santos:** Supervision, Conceptualization. **Pierre Olivier:** Writing – review & editing, Supervision. **Fausto Gallucci:** Writing – review & editing, Supervision, Resources, Conceptualization.

Declaration of competing interest

The authors declare that they have no known competing financial interests or personal relationships that could have appeared to influence the work reported in this paper.

Appendix A. Supplementary data

Supplementary data to this article can be found online at https://doi.org/10.1016/j.ijhydene.2024.05.308.

References

[1] IEA. Status of power system transformation. 2019. n.d.

[2] Hunter CA. Techno-economic analysis of long-duration energy storage and flexible power generation technologies to support high-variable renewable energy grids n. d.:vol. 26.
[3] IEA. Net. Zero by 2050 - a roadmap for the global energy sector. 2021. p. 224.
[4] ETN GLobal. ETN-R&D-Recommendation-Report-2021 edition. 2021.
[5] Wang Z, Wang Y, Afshan S, Hjalmarsson J. A review of metallic tanks for H2 storage with a view to application in future green shipping. Int J Hydrogen Energy 2021;46:6151–79. https://doi.org/10.1016/j.ijhydene.2020.11.168.
[6] Nazir H, Muthuswamy N, Louis C, Jose S, Prakash J, Buan ME, et al. Is the H2 economy realizable in the foreseeable future? Part II: H2 storage, transportation, and distribution. Int J Hydrogen Energy 2020;45:20693–708. https://doi.org/10.1016/j.ijhydene.2020.05.241.
[7] Hammad A, Dincer I. Analysis and assessment of an advanced hydrogen liquefaction system. Int J Hydrogen Energy 2018;43:1139–51. https://doi.org/10.1016/j.ijhydene.2017.10.158.
[8] Morlanés N, Katikaneni SP, Paglieri SN, Harale A, Solami B, Sarathy SM, et al. A technological roadmap to the ammonia energy economy: current state and missing technologies. Chem Eng J 2021;408:127310. https://doi.org/10.1016/j.cej.2020.127310.
[9] Asif M, Sidra Bibi S, Ahmed S, Irshad M, Shakir Hussain M, Zeb H, et al. Recent advances in green hydrogen production, storage and commercial-scale use via catalytic ammonia cracking. Chem Eng J 2023;473:145381. https://doi.org/10.1016/j.cej.2023.145381.
[10] Eppinger J, Huang K-W. Formic acid as a hydrogen energy carrier. ACS Energy Lett 2017;2:188–95. https://doi.org/10.1021/acsenergylett.6b00574.
[11] Valera-Medina A, Xiao H, Owen-Jones M, David WIF, Bowen PJ. Ammonia for power. Prog Energy Combust Sci 2018;69:63–102. https://doi.org/10.1016/j.pecs.2018.07.001.
[12] Zhao Y, Setzler BP, Wang J, Nash J, Wang T, Xu B, et al. An efficient direct ammonia fuel cell for affordable carbon-neutral transportation. Joule 2019;3:2472–84. https://doi.org/10.1016/j.joule.2019.07.005.
[13] Dias V, Pochet M, Contino F, Jeanmart H. Energy and economic costs of chemical storage. Front Mech Eng 2020;6:21. https://doi.org/10.3389/fmech.2020.00021.
[14] IEA. The future of hydrogen, vol. 203; 2019.
[15] Valera-Medina A, Amer-Hatem F, Azad AK, Dedoussi IC, de Joannon M, Fernandes RX, et al. Review on ammonia as a potential fuel: from synthesis to economics. Energy Fuels 2021;35:6964–7029. https://doi.org/10.1021/acs.energyfuels.0c03685.
[16] Okafor EC, Somarathne KDKA, Ratthanan R, Hayakawa A, Kudo T, Kurata O, et al. Control of NOx and other emissions in micro gas turbine combustors fuelled with mixtures of methane and ammonia. Combust Flame 2020;211:406–16. https://doi.org/10.1016/j.combustflame.2019.10.012.
[17] Ichikawa A, Hayakawa A, Kitagawa Y, Kunkuma Amila Somarathne KD, Kudo T, Kobayashi H. Laminar burning velocity and Markstein length of ammonia/hydrogen/air premixed flames at elevated pressures. Int J Hydrogen Energy 2015;40:9570–8. https://doi.org/10.1016/j.ijhydene.2015.04.024.
[18] Mitsubishi. Mitsubishi power commences development of world's first ammonia-fired 40MW class gas turbine system. https://power.mhi.com/news/20210301.html; 2021.
[19] GE and IHI sign agreement to develop ammonia fuels roadmap across asia. https://www.ge.com/news/press-releases/ge-and-ihi-sign-agreement-to-develop-ammonia-fuels-roadmap-across-asia; 2021.
[20] Bioche K, Bricteux L, Bertolino A, Parente A, Blondeau J. Large Eddy Simulation of rich ammonia/hydrogen/air combustion in a gas turbine burner. Int J Hydrogen Energy 2021;46:39548–62. https://doi.org/10.1016/j.ijhydene.2021.09.164.
[21] Li Z, Li S. Kinetics modeling of NOx emissions characteristics of a NH3/H2 fueled gas turbine combustor. Int J Hydrogen Energy 2021;46:4526–37. https://doi.org/10.1016/j.ijhydene.2020.11.024.
[22] Kurata O, Iki N, Matsunuma T, Inoue T, Tsujimura T, Furutani H, et al. Performances and emission characteristics of NH3–air and NH3CH4–air combustion gas-turbine power generations. Proc Combust Inst 2017;36:3351–9. https://doi.org/10.1016/j.proci.2016.07.088.
[23] Verkamp FJ, Hardin MC, Williams JR. Ammonia combustion properties and performance in gas-turbine burners. Symposium (International) on Combustion 1967;11:985–92. https://doi.org/10.1016/S0082-0784(67)80225-X.
[24] Valera-Medina A, Marsh R, Runyon J, Pugh D, Beasley P, Hughes T, et al. Ammonia–methane combustion in tangential swirl burners for gas turbine power generation. Appl Energy 2017;185:1362–71. https://doi.org/10.1016/j.apenergy.2016.02.073.
[25] Hussein NA, Valera-Medina A, Alsaegh AS. Ammonia- hydrogen combustion in a swirl burner with reduction of NOx emissions. Energy Proc 2019;158:2305–10. https://doi.org/10.1016/j.egypro.2019.01.265.
[26] Pugh D, Bowen P, Valera-Medina A, Giles A, Runyon J, Marsh R. Influence of steam addition and elevated ambient conditions on NOx reduction in a staged premixed swirling NH3/H2 flame. Proc Combust Inst 2019;37:5401–9. https://doi.org/10.1016/j.proci.2018.07.091.
[27] Xiao H, Valera-Medina A, Bowen P, Dooley S. 3D simulation of ammonia combustion in a lean premixed swirl burner. Energy Proc 2017;142:1294–9. https://doi.org/10.1016/j.egypro.2017.12.504.
[28] Kurata O. Pure ammonia combustion micro gas turbine system. 2019.
[29] Lee JH, Kim JH, Park JH, Kwon OC. Studies on properties of laminar premixed hydrogen-added ammonia/air flames for hydrogen production. Int J Hydrogen Energy 2010;35:1054–64. https://doi.org/10.1016/j.ijhydene.2009.11.071.
[30] Mounaïm-Rousselle C, Bréquigny P, Dumand C, Houillé S. Operating limits for ammonia fuel spark-ignition engine. Energies 2021;14:4141. https://doi.org/10.3390/en14144141.
[31] Hu X, Li J, Pan J, Zhang R, Wei H, Shu G. On combustion and emission characteristics of ammonia/hydrogen engines: emphasis on energy ratio and equivalence ratio. Fuel 2024;365:131183. https://doi.org/10.1016/j.fuel.2024.131183.
[32] Yan Y, Liu Z, Liu J. An evaluation of the conversion of gasoline and natural gas spark ignition engines to ammonia/hydrogen operation from the perspective of laminar flame speed. J Energy Resour Technol 2023;145:012302. https://doi.org/10.1115/1.4054754.
[33] Li J, Huang H, Kobayashi N, He Z, Nagai Y. Study on using hydrogen and ammonia as fuels: combustion characteristics and NO_x formation: hydrogen and ammonia as fuels. Int J Energy Res 2014;38:1214–23. https://doi.org/10.1002/er.3141.
[34] Port of Rotterdam. Large-Scale industrial ammonia cracking plant. 2023.
[35] Air liquide. Air Liquide ouvre la voie à la conversion d'ammoniac en hydrogène avec une nouvelle technologie de craquage. https://www.airliquide.com/fr/group/communiques-presse-actualites/23-03-2023/air-liquide-ouvre-la-voie-la-conversion-dammoniac-en-hydrogene-avec-une-nouvelle-technologie-de; 2023.
[36] Agency for Natural Resources and Energy. Overview of basic hydrogen strategy. 2023.
[37] Lamb KE, Dolan MD, Kennedy DF. Ammonia for hydrogen storage; A review of catalytic ammonia decomposition and hydrogen separation and purification. Int J Hydrogen Energy 2019;44:3580–93. https://doi.org/10.1016/j.ijhydene.2018.12.024.
[38] Lucentini I, Garcia X, Vendrell X, Llorca J. Review of the decomposition of ammonia to generate hydrogen. Ind Eng Chem Res 2021;60:18560–611. https://doi.org/10.1021/acs.iecr.1c00843.
[39] Chen C, Wu K, Ren H, Zhou C, Luo Y, Lin L, et al. Ru-based catalysts for ammonia decomposition: a mini-review. Energy Fuels 2021;35:11693–706. https://doi.org/10.1021/acs.energyfuels.1c01261.
[40] Cechetto V, Di Felice L, Gallucci F. Advances and perspectives of H_2 production from NH_3 decomposition in membrane reactors. Energy Fuels 2023;37:10775–98. https://doi.org/10.1021/acs.energyfuels.3c00760.
[41] Cechetto V, Di Felice L, Medrano JA, Makhloufi C, Zuniga J, Gallucci F. H2 production via ammonia decomposition in a catalytic membrane reactor. Fuel Process Technol 2021;216:106772. https://doi.org/10.1016/j.fuproc.2021.106772.
[42] Itoh N. Kinetic enhancement of ammonia decomposition as a chemical hydrogen carrier in palladium membrane reactor. Catal Today 2014;7.
[43] Liu J, Ju X, Tang C, Liu L, Li H, Chen P. High performance stainless-steel supported Pd membranes with a finger-like and gap structure and its application in NH3 decomposition membrane reactor. Chem Eng J 2020;388:124245. https://doi.org/10.1016/j.cej.2020.124245.
[44] Park Y, Cha J, Oh H-T, Lee T, Lee SH, Park MG, et al. A catalytic composite membrane reactor system for hydrogen production from ammonia using steam as a sweep gas. J Membr Sci 2020;614:118483. https://doi.org/10.1016/j.memsci.2020.118483.
[45] Cerrillo JL, Morlanés N, Kulkarni SR, Realpe N, Ramírez A, Katikaneni SP, et al. High purity, self-sustained, pressurized hydrogen production from ammonia in a catalytic membrane reactor. Chem Eng J 2021:134310. https://doi.org/10.1016/j.cej.2021.134310.
[46] Lim D, Lee A, Kim A, Haider J, Mikulčić H, Brigljević B, et al. A 4E feasibility analysis of an on-site, ammonia sourced, hydrogen refueling station. J Clean Prod 2022;363:132356. https://doi.org/10.1016/j.jclepro.2022.132356.
[47] Makhloufi C. Large-scale decomposition of green ammonia for pure hydrogen production, vol. 11; 2021.
[48] Nasharuddin R, Zhu M, Zhang Z, Zhang D. A technoeconomic analysis of centralised and distributed processes of ammonia dissociation to hydrogen for fuel cell vehicle applications. Int J Hydrogen Energy 2019;44:14445–55. https://doi.org/10.1016/j.ijhydene.2019.03.274.
[49] Cesaro Z, Ives M, Nayak-Luke R, Mason M, Bañares-Alcántara R. Ammonia to power: forecasting the levelized cost of electricity from green ammonia in large-scale power plants. Appl Energy 2021;282:116009. https://doi.org/10.1016/j.apenergy.2020.116009.
[50] Manzolini G, Macchi E, Binotti M, Gazzani M. Integration of SEWGS for carbon capture in natural gas combined cycle. Part B: reference case comparison. Int J Greenh Gas Control 2011;5:214–25. https://doi.org/10.1016/j.ijggc.2010.08.007.
[51] Klerke A, Christensen CH, Nørskov JK, Vegge T. Ammonia for hydrogen storage: challenges and opportunities. J Mater Chem 2008;18:2304. https://doi.org/10.1039/b720020j.
[52] Fernandez E, Helmi A, Coenen K, Melendez J, Viviente JL, Pacheco Tanaka DA, et al. Development of thin Pd–Ag supported membranes for fluidized bed membrane reactors including WGS related gases. Int J Hydrogen Energy 2015;40:3506–19. https://doi.org/10.1016/j.ijhydene.2014.08.074.
[53] de Nooijer N, Gallucci F, Pellizzari E, Melendez J, Pacheco Tanaka DA, Manzolini G, et al. On concentration polarisation in a fluidized bed membrane reactor for biogas steam reforming: modelling and experimental validation. Chem Eng J 2018;348:232–43. https://doi.org/10.1016/j.cej.2018.04.205.
[54] Helmi A, Voncken RJW, Raijmakers AJ, Roghair I, Gallucci F, van Sint Annaland M. On concentration polarization in fluidized bed membrane reactors. Chem Eng J 2018;332:464–78. https://doi.org/10.1016/j.cej.2017.09.045.
[55] Chen W-H, Hsia M-H, Lin Y-L, Chi Y-H, Yang C-C. Hydrogen permeation and recovery from H2–N2 gas mixtures by Pd membranes with high permeance. Int J Hydrogen Energy 2013;38:14730–42. https://doi.org/10.1016/j.ijhydene.2013.08.086.
[56] Helmi A, Voncken RJW, Raijmakers AJ, Roghair I, Gallucci F, van Sint Annaland M. On concentration polarization in fluidized bed membrane reactors. Chem Eng J 2018;332:464–78. https://doi.org/10.1016/j.cej.2017.09.045.

[57] Nordio M, Soresi S, Manzolini G, Melendez J, Van Sint Annaland M, Pacheco Tanaka DA, et al. Effect of sweep gas on hydrogen permeation of supported Pd membranes: experimental and modeling. Int J Hydrogen Energy 2019;44:4228–39. https://doi.org/10.1016/j.ijhydene.2018.12.137.
[58] de Nooijer N, Gallucci F, Pellizzari E, Melendez J, Pacheco Tanaka DA, Manzolini G, et al. On concentration polarisation in a fluidized bed membrane reactor for biogas steam reforming: modelling and experimental validation. Chem Eng J 2018;348:232–43. https://doi.org/10.1016/j.cej.2018.04.205.
[59] Richard S, Ramirez Santos A, Gallucci F. PEM gensets using membrane reactors technologies: an economic comparison among different e-fuels. Int J Hydrogen Energy 2023;S0360319923032913. https://doi.org/10.1016/j.ijhydene.2023.06.312.
[60] Di Carlo A, Vecchione L, Del Prete Z. Ammonia decomposition over commercial Ru/Al2O3 catalyst: an experimental evaluation at different operative pressures and temperatures. Int J Hydrogen Energy 2014;39:808–14. https://doi.org/10.1016/j.ijhydene.2013.10.110.
[61] Chiuta S, Everson RC, Everson RC, Neomagus HWJP, Neomagus HWJP, Bessarabov DG. Ammonia decomposition for decentralized hydrogen production in microchannel reactors: experiments and CFD simulations. In: Sankir M, Sankir ND, editors. Hydrogen production technologies. Hoboken, NJ, USA: John Wiley & Sons, Inc.; 2017. p. 77–111. https://doi.org/10.1002/9781119283676.ch2.
[62] Spallina V, Pandolfo D, Battistella A, Romano MC, Van Sint Annaland M, Gallucci F. Techno-economic assessment of membrane assisted fluidized bed reactors for pure H 2 production with CO 2 capture. Energy Convers Manag 2016;120:257–73. https://doi.org/10.1016/j.enconman.2016.04.073.
[63] Medrano JA, Llosa-Tanco MA, Cechetto V, Pacheco-Tanaka DA, Gallucci F. Upgrading biogas with novel composite carbon molecular sieve (CCMS) membranes: experimental and techno-economic assessment. Chem Eng J 2020;394:124957. https://doi.org/10.1016/j.cej.2020.124957.
[64] Manzolini G, Macchi E, Gazzani M. CO2 capture in natural gas combined cycle with SEWGS. Part B: economic assessment. Int J Greenh Gas Control 2013;12:502–9. https://doi.org/10.1016/j.ijggc.2012.06.021.
[65] Gerdes K, Summers W, Wimer J. Quality guidelines for energy system studies: cost estimation methodology for NETL assessments of power plant performance. https://doi.org/10.2172/1513278; 2011.
[66] Turton R, editor. Analysis, synthesis, and design of chemical processes. fifth ed. Boston: Prentice Hall; 2018.
[67] DOE/NETL. Cost and performance baseline for fosssil energy plants. 2007.
[68] Neveux T, Authier O, Moullec YL. Estimation technico-économique d'innovations technologiques en génie des procédés, vol. 32; 2020.
[69] AACE. 16R-90: conducting technical and economic evaluations - as applied for the process and utility Industries, vol. 11; 1991.
[70] Haldor Topsoe A/S. Topsoes ammonia cracking technology – delivering green hydrogen. 2021.
[71] Wismann ST, Engbæk JS, Vendelbo SB, Bendixen FB, Eriksen WL, Aasberg-Petersen K, et al. Electrified methane reforming: a compact approach to greener industrial hydrogen production. Science 2019;364:756–9. https://doi.org/10.1126/science.aaw8775.
[72] Advanced materials and reactors for Energy storage through ammonia 2023. https://arenha.eu/. [Accessed 23 October 2023].
[73] Valentini A. Green shift to create 1 billion tonne 'green ammonia' market?, vol. 6; 2020.
[74] Fasihi M, Weiss R, Savolainen J, Breyer C. Global potential of green ammonia based on hybrid PV-wind power plants. Appl Energy 2021;294:116170. https://doi.org/10.1016/j.apenergy.2020.116170.
[75] Morgan. Techno-economic feasibility study of ammonia plants powered by offshore. Wind 2021. https://doi.org/10.7275/11KT-3F59.
[76] Osman O, Sgouridis S, Sleptchenko A. Scaling the production of renewable ammonia: a techno-economic optimization applied in regions with high insolation. J Clean Prod 2020;271:121627. https://doi.org/10.1016/j.jclepro.2020.121627.
[77] Nayak-Luke RM, Forbes C, Cesaro Z, Bañares-Alcántara R, Rouwenhorst KHR. Techno-economic aspects of production, storage and distribution of ammonia. Techno-economic challenges of green ammonia as an energy vector. Elsevier; 2021. p. 191–207. https://doi.org/10.1016/B978-0-12-820560-0.00008-4.
[78] Yoshida M, Ogawa T, Imamura Y, Ishihara KN. Economies of scale in ammonia synthesis loops embedded with iron- and ruthenium-based catalysts. Int J Hydrogen Energy 2021;46:28840–54. https://doi.org/10.1016/j.ijhydene.2020.12.081.
[79] Atsbha TA, Yoon T, Yoo B-H, Lee C-J. Techno-economic and environmental analysis for direct catalytic conversion of CO2 to methanol and liquid/high-calorie-SNG fuels. Catalysts 2021;11:687. https://doi.org/10.3390/catal11060687.
[80] Viviente JL. FluidCell : advanced m-CHP fuel cell system based on a novel bioethanol fluidized bed membrane reformer. 2018.
[81] Fluid Cell Project n.d. https://www.fluidcell.eu/(accessed April 3, 2023).
[82] MACBETH n.d. https://www.macbeth-project.eu/. [Accessed 3 February 2023].
[83] Nordio M, Wassie SA, Van Sint Annaland M, Pacheco Tanaka DA, Viviente Sole JL, Gallucci F. Techno-economic evaluation on a hybrid technology for low hydrogen concentration separation and purification from natural gas grid. Int J Hydrogen Energy 2021;46:23417–35. https://doi.org/10.1016/j.ijhydene.2020.05.009.
[84] Bellotti D, Rivarolo M, Magistri L. A comparative techno-economic and sensitivity analysis of Power-to-X processes from different energy sources. Energy Convers Manag 2022;260:115565. https://doi.org/10.1016/j.enconman.2022.115565.
[85] Manzolini G, Sanchez Fernandez E, Rezvani S, Macchi E, Goetheer ELV, Vlugt TJH. Economic assessment of novel amine based CO2 capture technologies integrated in power plants based on European Benchmarking Task Force methodology. Appl Energy 2015;138:546–58. https://doi.org/10.1016/j.apenergy.2014.04.066.
[86] Sayas S, Morlanés N, Katikaneni SP, Harale A, Solami B, Gascon J. High pressure ammonia decomposition on Ru–K/CaO catalysts. Catal Sci Technol 2020;10:5027–35. https://doi.org/10.1039/D0CY00686F.
[87] Im Y, Muroyama H, Matsui T, Eguchi K. Ammonia decomposition over nickel catalysts supported on alkaline earth metal aluminate for H2 production. Int J Hydrogen Energy 2020;45:26979–88. https://doi.org/10.1016/j.ijhydene.2020.07.014.
[88] Sayas S, Morlanés N, Katikaneni SP, Harale A, Solami B, Gascon J. High pressure ammonia decomposition on Ru–K/CaO catalysts. Catal Sci Technol 2020;10:5027–35. https://doi.org/10.1039/D0CY00686F.
[89] Sitar R, Shah J, Zhang Z, Wikoff H, Way JD, Wolden CA. Compact ammonia reforming at low temperature using catalytic membrane reactors. J Membr Sci 2022;644:120147. https://doi.org/10.1016/j.memsci.2021.120147.
[90] Chen W-H, Chou W-S, Chein R-Y, Hoang AT, Juan JC. Multiple-objective optimization on ammonia decomposition using membrane reactor. Int J Hydrogen Energy 2023. https://doi.org/10.1016/j.ijhydene.2023.05.081. S0360319923023339.
[91] Abu El Hawa HW, Lundin S-TB, Paglieri SN, Harale A, Douglas Way J. The influence of heat treatment on the thermal stability of Pd composite membranes. J Membr Sci 2015;494:113–20. https://doi.org/10.1016/j.memsci.2015.07.021.
[92] Lee S, Kim HS, Park J, Kang BM, Cho C-H, Lim H, et al. Scenario-based techno-economic analysis of steam methane reforming process for hydrogen production. Appl Sci 2021;11:6021. https://doi.org/10.3390/app11136021.
[93] Helmi A, Gallucci F, van Sint Annaland M. Resource scarcity in palladium membrane applications for carbon capture in integrated gasification combined cycle units. Int J Hydrogen Energy 2014;39:10498–506. https://doi.org/10.1016/j.ijhydene.2014.05.009.
[94] Satistica. Mine production of palladium worldwide in 2022, by country n.d. https://www.statista.com/statistics/273647/global-mine-production-of-palladium/. [Accessed 19 April 2023].
[95] Statista. Demand for ruthenium worldwide from 2010 to 2023 n.d. https://www.statista.com/statistics/591965/demand-for-ruthenium-worldwide/. [Accessed 17 November 2023].